HARMONIC GENERATION IN THE SOUND FIELD OF A 3 MHz, 1/2 INCH DIAMETER PLANE PISTON SOURCE

BY

WING KONG LAW

B.S., University of Rochester, 1978

THESIS

Submitted in partial fulfillment of the requirements
for the degree of Master of Science in Electrical Engineering
in the Graduate College of the
University of Illinois at Urbana-Champaing, 1980

Urbana, Illinois

ACKNOWLEDGEMENT

The author wishes to express his grateful appreciation to his advisors, Dr. Floyd Dunn and Dr. Leon Frizzell for their encouragement and guidance throughout this investigation. Appreciation is also extended to Mr. Joseph Cobb for his technical assistance. Also, the author acknowledges gratefully the support from a NSF grant, NSF ENG 77-20934.

TABLE OF CONTENTS

	Page
ACKNOWLEDGEMENT	iii
LIST OF TABLES	v
LIST OF FIGURES	vi
INTRODUCTION	1
THEORY	4
APPARATUS	18
CALIBRATION	24
DATA AND DISCUSSION	34
COMPARISON WITH THEORY	50
SUMMARY	56
APPENDIX	57
REFERENCES	65

LIST OF TABLES

Page

1. K_a and Y for frequencies used in calibration 28

2. Hydrophone sensitivity and error margin. 32

3. Half power beam width for the first three harmonics at different source pressures 46

4. Discontinuity distances for the source levels used in this project. 50

5. Intensity transmission coefficient of filtering plate. 63

LIST OF FIGURES

Page

1. Distortion of an originally sinusoidal wave form. 5
2. Discontinuity distance in water vs. frequency for different source intensities 7
3. Locus of points which satisfy the relation $\Phi = \sigma \sin \Phi$ 9
4. Fourier coefficient B_n for distorted wave at different σ values 10
5. Magnitude of second and third harmonic relative to fundamental 11
6. Normalized fundamental component for various values of $\alpha_o L$ 14
7. Normalized second harmonic for various values of $\alpha_o L$ 15
8. Normalized third harmonic for various values of $\alpha_o L$ 16
9. Block diagram of apparatus 19
10. Source transducer housing and mounting 21
11. Hydrophone construction 23
12. System for total power measurement 25
13. Total acoustical power vs. square of source voltage 27
14. Beam patterns of calibrating fields 30
15. Hydrophone output voltage vs. source voltage at the calibration positions 31
16. Harmonic pressure magnitude at different distances from source 36
17. Relative harmonic magnitude along axis of transducer 38
18. Axial harmonic magnitude vs. source pressure at 12 cm from source 40

LIST OF FIGURES (continued)

Page

19. Deviation of fundamental magnitude from linearity at different source pressures 41

20. Relative harmonic magnitude vs. source pressure at 12 cm from source 42

21. Beam patterns of fundamental and harmonics at source pressures of 1.56 atm measured at 12 cm from source 43

22. Normailzed transaxial beam profile for the first three harmonics at two different source pressures 45

23. Spatially averaged harmonic pressure magnitude vs. source pressure 48

24. Spatially averaged relative harmonic magnitude vs. source pressure 52

25. $P_n(x)/P_1(x)$ along axis, theory and measurement 53

26. P_n/P_1 vs. source pressure at 12 cm, theory and measurement 54

27. Spatially averaged P_n/P_1 at 12 cm, theory and measurement 55

28. Spatial sum of harmonic intensities vs. total acoustical power at the source 59

29. Sound power transmission through a half wavelength plate at normal incidence 61

30. Frequency of maximum transmission of a filtering plate vs. angle of incidence 62

CHAPTER I: INTRODUCTION

The acoustic wave equation describing the propagation of noninfinitismal (finite amplitude) waves in fluids is nonlinear. As a result, an originally sinusoidal wave is distorted as it propagates. Higher harmonics are generated at the expense of the fundamental frequency component. The presence of higher harmonics leads to an increase in the rate of energy absorption (Keck and Beyer, 1960); the depletion of the fundamental and the increased space rate of absorption leads to the saturation of acoustical power (Shooter et al., 1974) and to a change of beam shape (Lockwood et al., 1973). The amount of distortion in an acoustic wave depends upon several factors, including the 1) frequency, 2) source intensity, 3) distance from the source, 4) nonlinear parameter of the medium, and 5) absorption in the medium.

In general, an increase in the first four factors increases the distortion, while increasing the fifth factor has the opposite effect. Thus, depending upon the combination of these factors, a wave can be regarded as of infinitesimal amplitude, so that the concepts of linear acoustics may apply, or it must be regarded as of finite amplitude and treated accordingly. In the area of biomedical ultrasound, the frequency-intensity-distance combinations often result in a borderline case, where care must be exercised to determine the appropriate description of the sound field.

Reasonable theoretical treatments are available to describe finite amplitude plane waves. However, a commonly employed source of

ultrasound is the circular plane piston, for which no simple complete theoretical description yet exists for the finite amplitude wave generated. Depending upon the size of the source and the distance at which measurements are made, such fields can sometimes be approximated as finite amplitude plane waves and the plane wave theory can be applied. However, it is not always clear when such an approximation can be made.

The project described here was aimed at developing a reliable technique for the measurement of the harmonic content in an ultrasonic wave. It is expected that through direct measurements, the gap in knowledge between the idealized concept of plane finite amplitude waves and the waves due to a piston source can be filled. For this purpose, a small size (2 mm diameter) piezoelectric probe was constructed and calibrated against a steel ball radiometer. The calibrated probe was then applied to measure the field generated by a 3.2 MHz, ½ inch diameter piston source. The results of the measurements are presented in this thesis and compared to those predicted by plane wave finite amplitude theory. Three cases were investigated:

1) Axial measurements: The magnitude of the first three harmonics was measured at different distances from the source (4 cm to 15 cm) along the axis of the source transducer.

2) Transaxial measurements: The harmonic content transverse to the main axis was measured at the near field/far field transition point (12 cm from the source). The beam profile of the first three harmonics and their change with source intensity are presented.

3) Spatial average harmonic content: The harmonic content of the sound beam was averaged over an area equal to that of the source and compared with that predicted by plane wave theory.

The spacially averaged harmonic content agrees approximately with the plane wave theory up to a source acoustic pressure of two atmospheres. The axial harmonic content of the particular piston source was found to be greater than that predicted by a plane wave theory.

CHAPTER II: THEORY

A. Finite amplitude effect, plane wave theory

Finite amplitude sound waves occupy the amplitude range between waves of infinitesimal amplitude and waves whose amplitude is sufficiently large to form a physical discontinuity, i.e. a shock front. A finite amplitude sound wave propagating through a fluid medium is distorted due to the nonlinearity in the wave equation and from the nonlinearity of the equation of state of the medium.

For liquids, the following assumed equation of state is often used (Beyer, Nonlinear Acoustics):

$$P = P_o + A(\rho-\rho_o/\rho_o) + B/2(\rho-\rho_o/\rho_o)^2 \qquad (1)$$

where $A = \rho_o(\partial P/\partial\rho)_{\rho=\rho_o}$, $B = \rho_o^2(\partial^2 P/\partial\rho^2)_{\rho=\rho_o}$,

P is the acoustic pressure, ρ is the density, and the zreo subscripts refer to the parameter values of the undisturbed medium. Using the above equation of state, Eq. (1), the phase velocity is (Beyer, Nonlinear Acoustics) $c = c_o + (B/2A + 1)\mu$, accurate to the first order in μ, where μ is the particle velocity and c_o is the velocity of the sound wave at infinitesimal amplitude. Different points along the waveform with different particle velocity values will therefore exhibit different local sound speeds. Points with large positive particle velocities will travel faster than the wave as a whole and points with negative particle velocity will be retarded. This process is illustrated in Fig. 1.

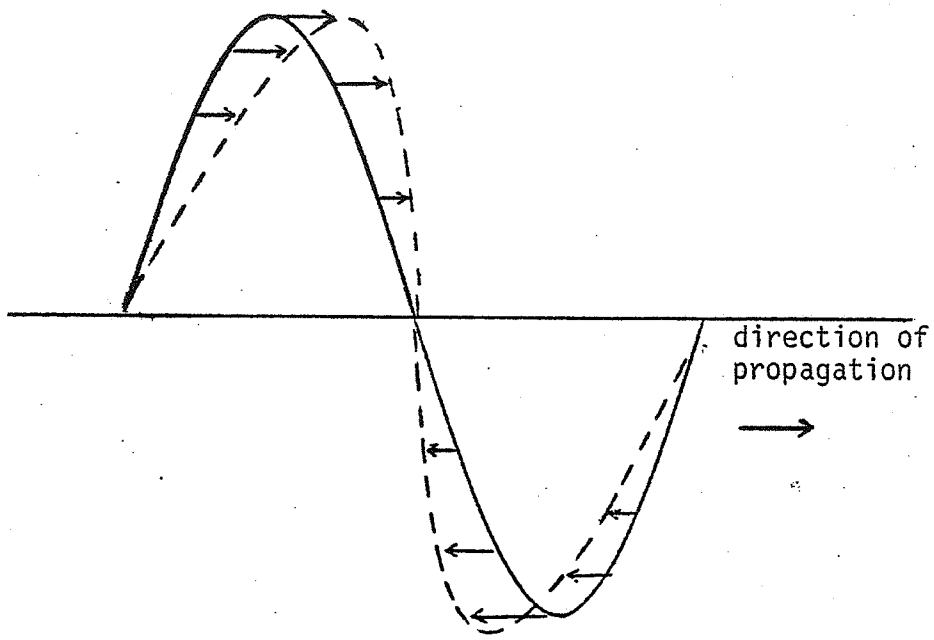

Figure 1. Distortion of an originally sinusoidal waveform.

Such distortion is a cumulative process. If the wave is allowed to travel far enough, the peak will eventually catch up with the axis crossing point of the wave, forming a physical discontinuity. The distance from the sound source at which such a discontinuity first occurs is called the "discontinuity distance", L, and is given by (Beyer, Nonlinear Acoustics)

$$L = c_o^2/[(1+B/2A)\omega\mu_o] \tag{2}$$

where c_o is the infinitesimal amplitude phase velocity, ω is the angular frequency, and μ_o is the particle velocity at the source. Figure 2 is a plot of the discontinuity distance versus frequency for a number of source intensities. However, it must be borne in mind that L is only a theoretical quantity. In a real medium, dissipation is present and tends to limit the formation of shocks. Thus a discontinuity is never formed.

The distorted waveform can be expressed in terms of a sum of harmonics by Fourier analysis as

$$\mu = \mu_o \sum_{n=1}^{\infty} B_n \sin[n(\omega t - kx)] \tag{3}$$

where μ is the particle velocity, k is the wave number, B_n is the Fourier coefficient, and n is the harmonic number. For a medium which has negligible absorption, B_n is given by (Blackstock, 1966)

$$B_n = [2/n\pi \sin(\Psi|_{y=0})] + [2/n\pi\sigma \int_{\Psi|_{y=0}}^{\pi} \cos n(\Psi - \sigma\sin\Psi)\, d\Psi] \tag{4}$$

Figure 2. Discontinuity Distance vs. Frequency for Different Source Intensities(W/cm^2) in Water (B/A = 5).

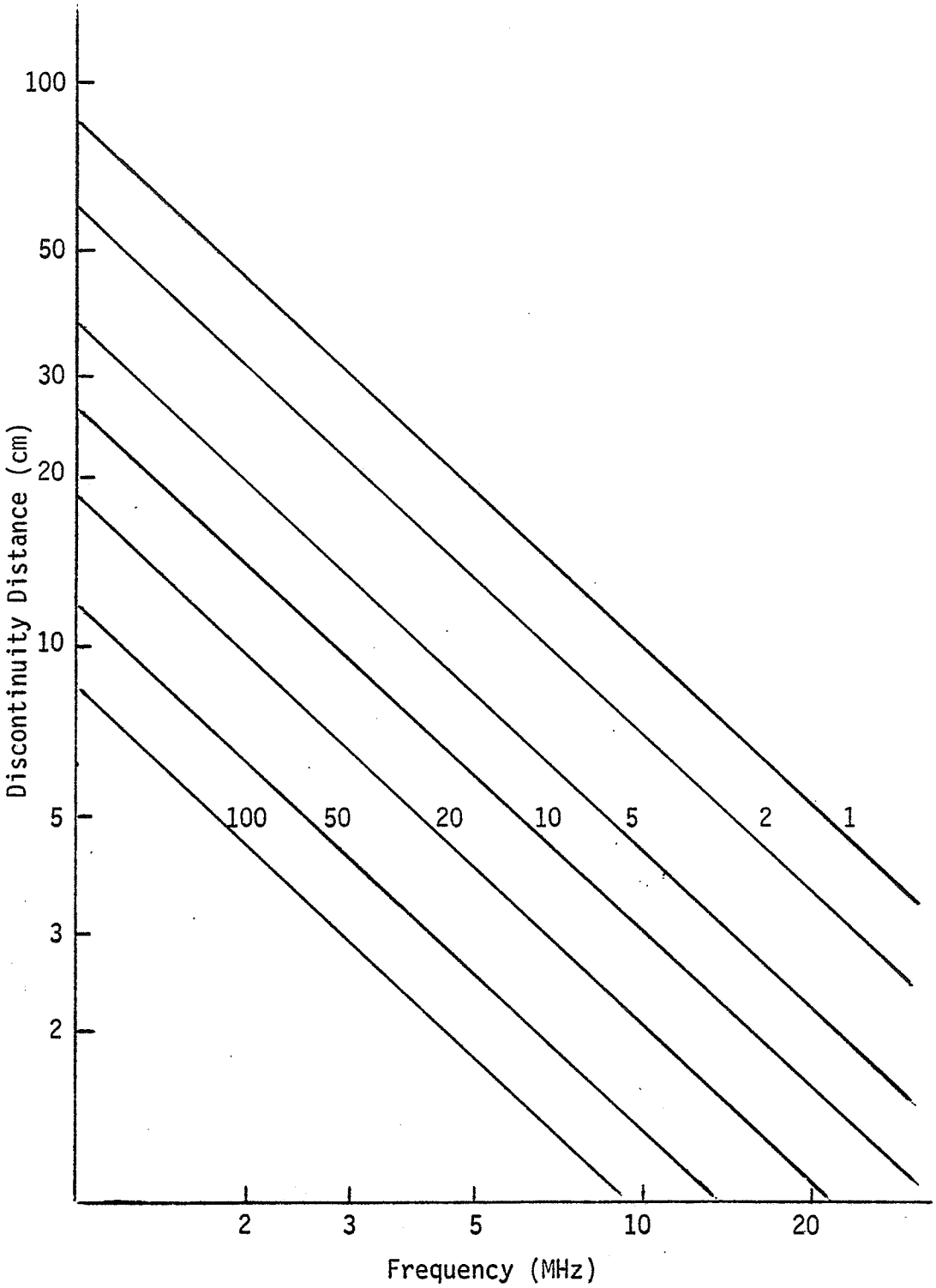

where I and y are intermediate variables, with $y = \Phi - \sigma\sin\Phi$, and σ = X/L = $\frac{\text{Distance from source at which waveform is measured}}{\text{Distance from source at which discontinuity is predicted to occur}}$.

To evaluate $\Phi\big|_{y=0}$, we have to solve the equation $y = 0$, i.e. $\Phi = \sigma\sin\Phi$. A solution is plotted in Figure 3. B_n values calculated by this method are shown in Figure 4, for n equal to one, two and three. As seen from the plot, the higher harmonics increase in magnitude with distance while the fundamental frequency component decreases in magnitude, indicating a transfer of energy from the fundamental to the higher harmonics. At $\sigma = 1$, i.e., $X = L$, the fundamental has lost 10% of its amplitude to the harmonics. At $\sigma = 3$, the fundamental has lost 50% of its original magnitude. The second and third harmonics have peaks around $\sigma = 1.3$. At this point, the rate of energy gain (due to transfer of energy from the fundamental) equals the rate of energy lost (transfer of energy to even higher harmonics).

Figure 4 can be replotted in the form B_n/B_1 vs. σ to illustrate the change of wave shape with distance, as shown in Figure 5. If the median has no loss, a true sawtooth wave will develop which has as its Fourier coefficients $B_n/B_1 = 1/n$, so that $B_2/B_1 = 0.5$, $B_3/B_1 = 0.33$, $B_4/B_1 = 0.25$, etc. From Figure 6, one observes that B_n/B_1 increases with distance, and approaches that of a sawtooth wave at $\sigma = 3$.

For σ less than unity, Eq. 3 can be reduced to the form

$$B_n = 2J_n(n\sigma)/n\sigma \qquad (5)$$

(Blackstock, 1966), where J_n is the Bessel function of the first kind

Figure 3. Locus of Points which Satisfy the Relation $\Phi = \sigma \sin \Phi$.

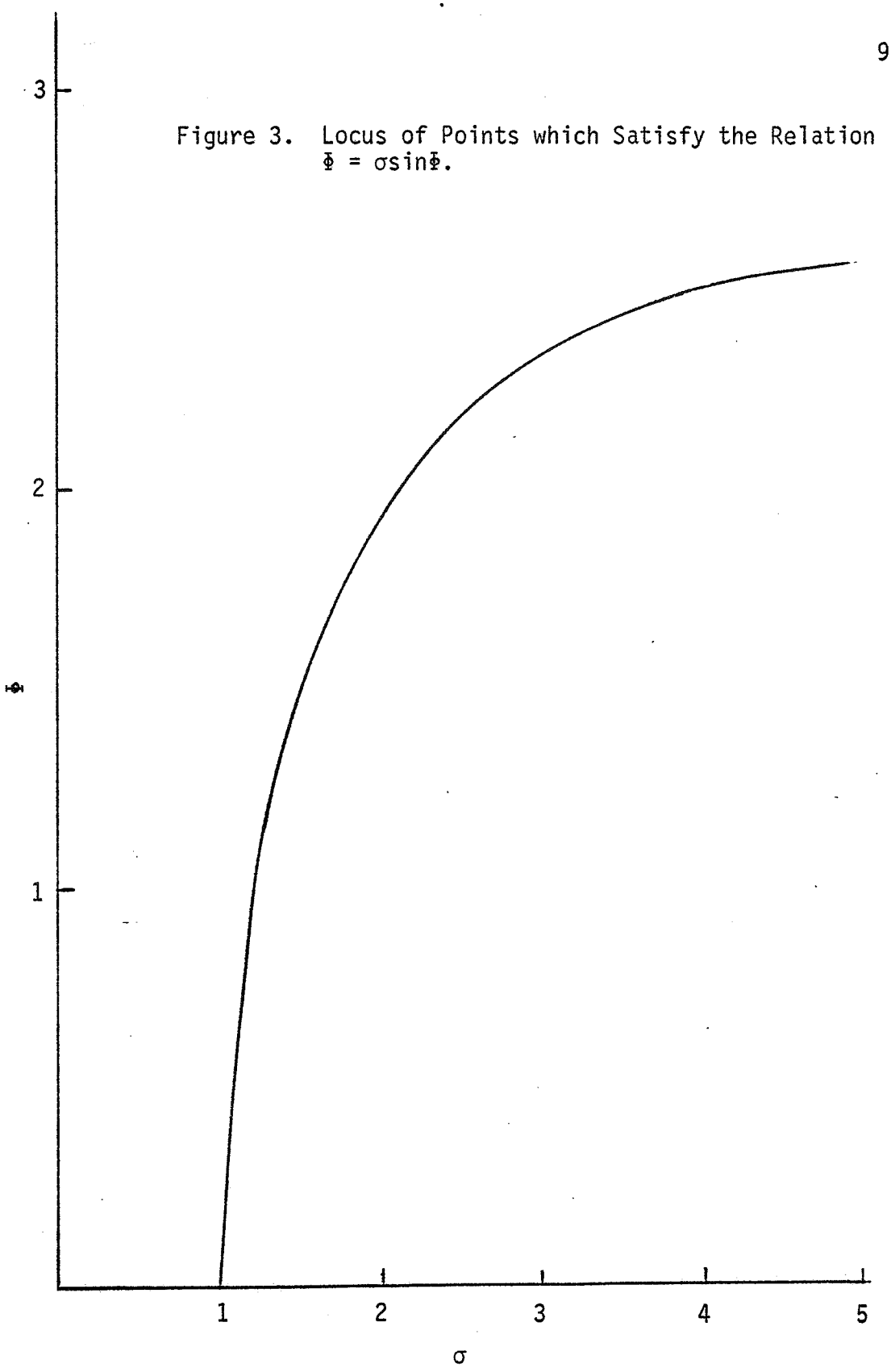

Figure 4. Fourier Coefficient for Distorted Wave at Different σ Values.

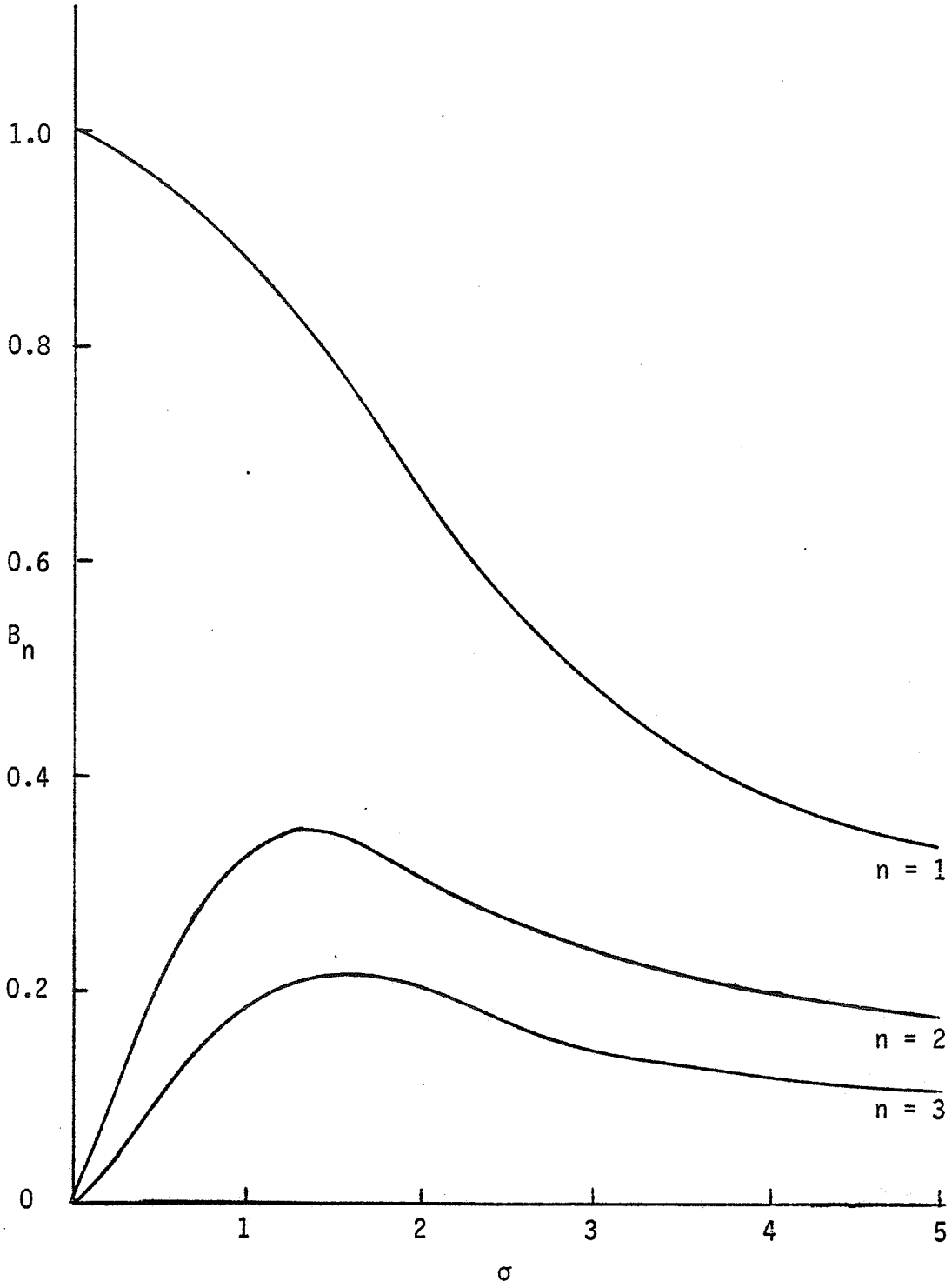

Figure 5. Magnitude of Second and Third Harmonic Components Relative to the Fundamental.

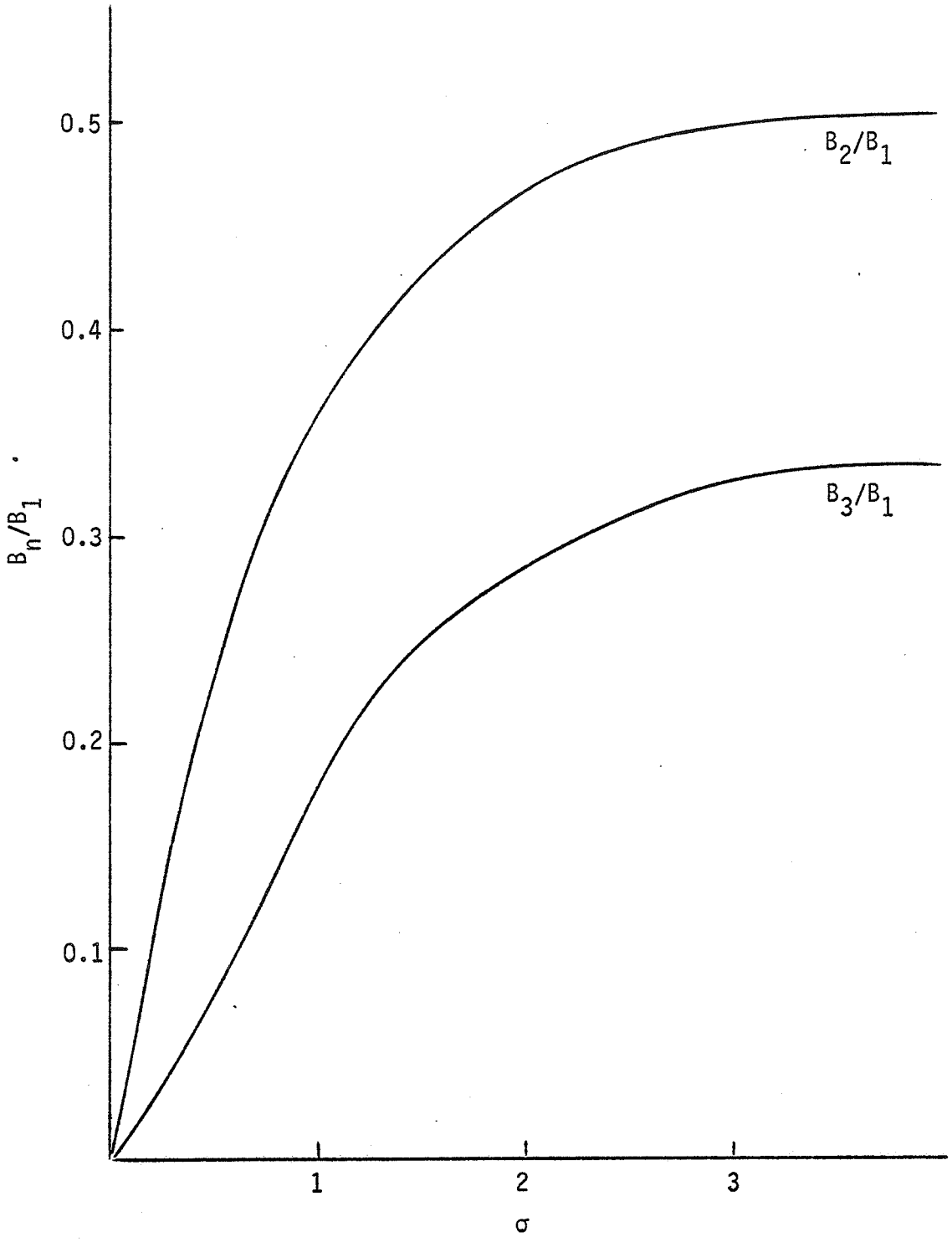

of order n. By expanding the Bessel function in a power series and dropping higher order terms, this equation can be reduced to give the second harmonic pressure magnitude as

$$P_2(x) = \pi[(1+B/2A)/(\rho_o c_o^3)]fxp_1^2(0) \qquad (6)$$

and the third harmonic pressure magnitude as

$$P_3(x) = 3[\pi(1+B/2A)/\rho_o c_o^3]^2 f^2 x^2 p_1^3(0) \qquad (7)$$

where $P_1(0)$ is the source pressure amplitude and f is the frequency. These approximate equations are valid only for small values of the argument of the Bessel function, i.e. $n\sigma \ll 1$. Under these conditions, the second harmonic increases with x and the square of the source pressure. The third harmonic increases with the square of the distance and the third power of source pressure.

Throughout the discussion so far, the absorption of the medium has been neglected. Theoretical work describing finite amplitude effects with consideration of absorption has been difficult and labored. The theories, which are usually based on equations approximating the exact differential equations, have a rather limited range of reliability. An alternate route would be to use numerical methods.

For the purpose of comparing experimental results in this project with theory, the computation developed by Cook (Cook, 1962) was used. The method of computation, in his own words, is as follows:

"The wave was allowed to distort while it propagates through a

small interval, and then was corrected for absorption. This wave of new shape was then allowed to distort and be absorbed. By assuming that no discontinuity of the wave shape is formed because of absorption, one may calculate by this continuing process the shape of the wave at all distances. Although the absorption and generation of the harmonics are treated independently in each small interval, the end result contains the interaction between absorption and generation mechanisms." Figures 6, 7 and 8 are results of his computations. An f^2 dependence of absorption was assumed in his calculations.

The infinitesimal amplitude absorption coefficient (α_0) for water at 3MHz is about 2.5×10^{-3} np/cm. If the discontinuity distance is 10 cm, $\alpha_0 L$ would be about 0.025. With $\alpha_0 L$ around this value, the magnitude of the first three harmonics can be very well approximated by the absorptionless theory, as is evident from a comparison of Figures 6, 7 and 8 with Figure 4.

B. Piston Sources

Theoretical analyses of finite amplitude effects often use the idealized concept of the plane wave. However, the standard device used to produce ultrasound is often a plane piston transducer. Because of diffraction effects, the distribution of intensity in the near field of a piston source is rather complex. In the infinitesimal amplitude case, the axial pressure $|p|$ of a piston source is given by (Kinsler and Frey, Fundamentals of Acoustics) $|p| = 2P_0 e^{-\alpha x} |\sin k/2(x_a - x)|$ where $x_a = \sqrt{x^2 + a^2}$, a is the radius of the piston, x is the distance

Figure 6. Normalized Fundamental Component for Various Values of $\alpha_o L$. $P_1(0)$ is Acoustic Pressure at the Source, $P_1(\sigma)$ is Acoustic Pressure at σ. (After B. Cook, 1962).

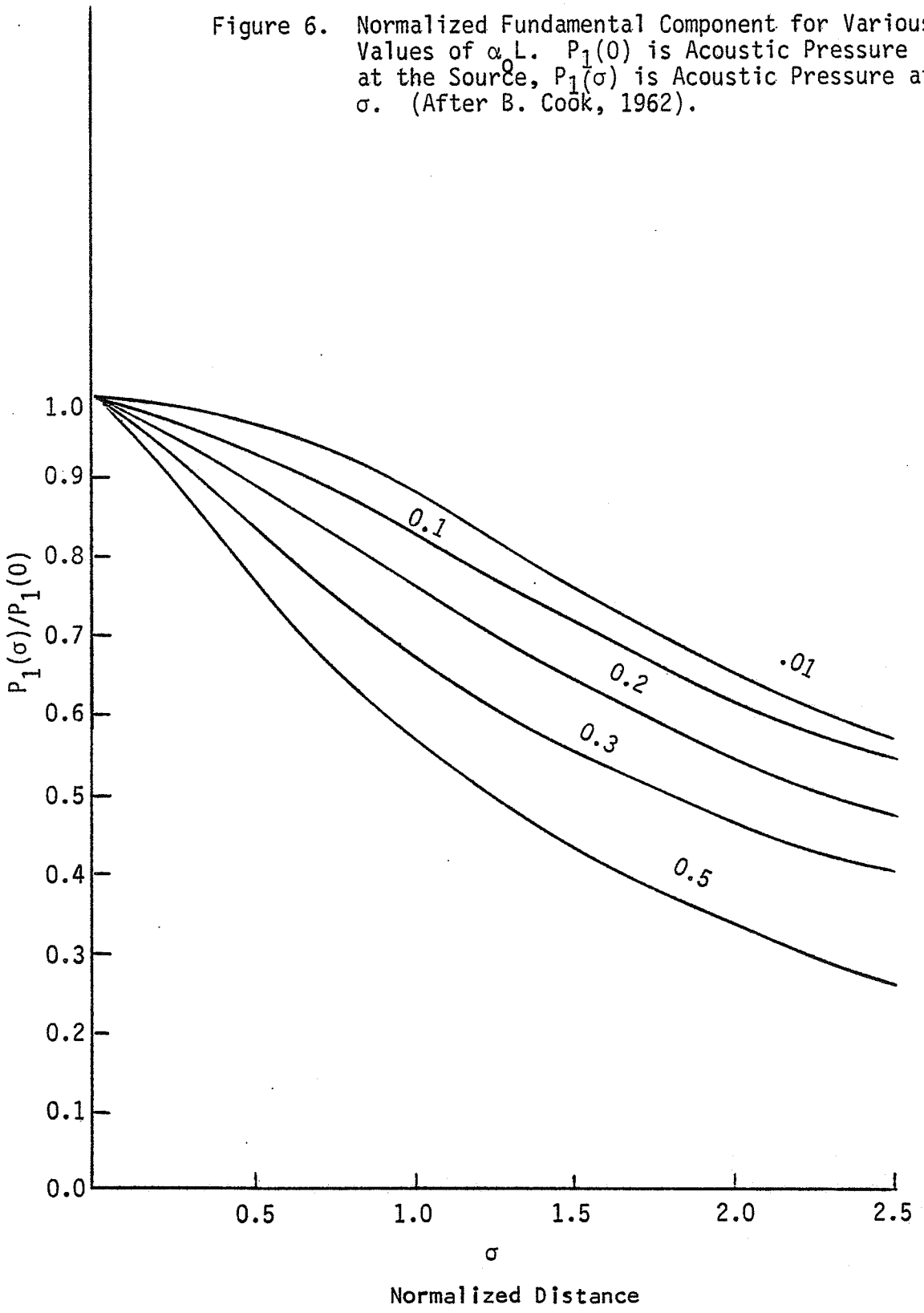

Figure 7. Normalized Second Harmonic Component For Various Values of $\alpha_o L$ (After B. Cook, 1962).

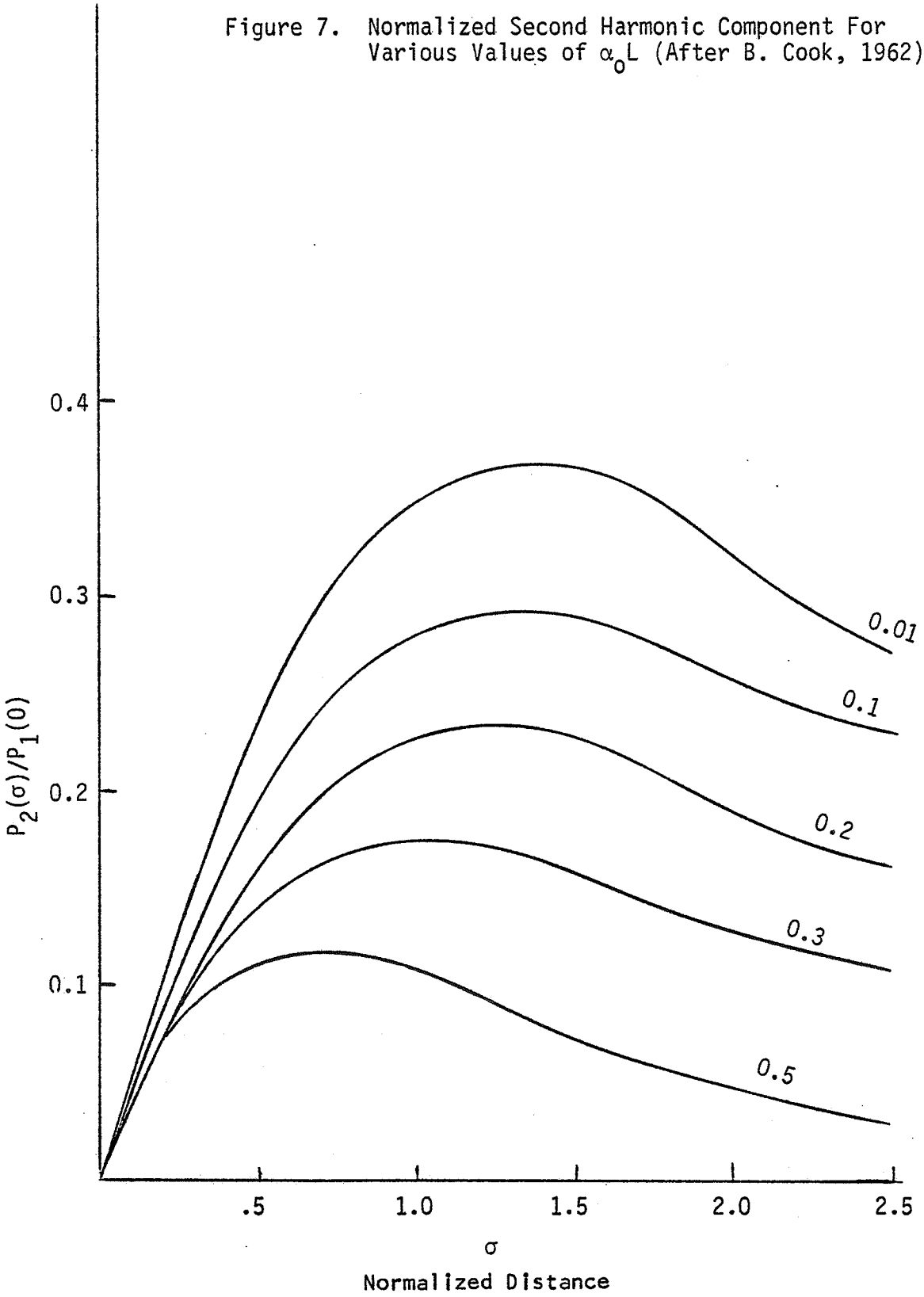

Figure 8. Normalized Third Harmonic Component For Various Values of $\alpha_o L$ (After B. Cook, 1962).

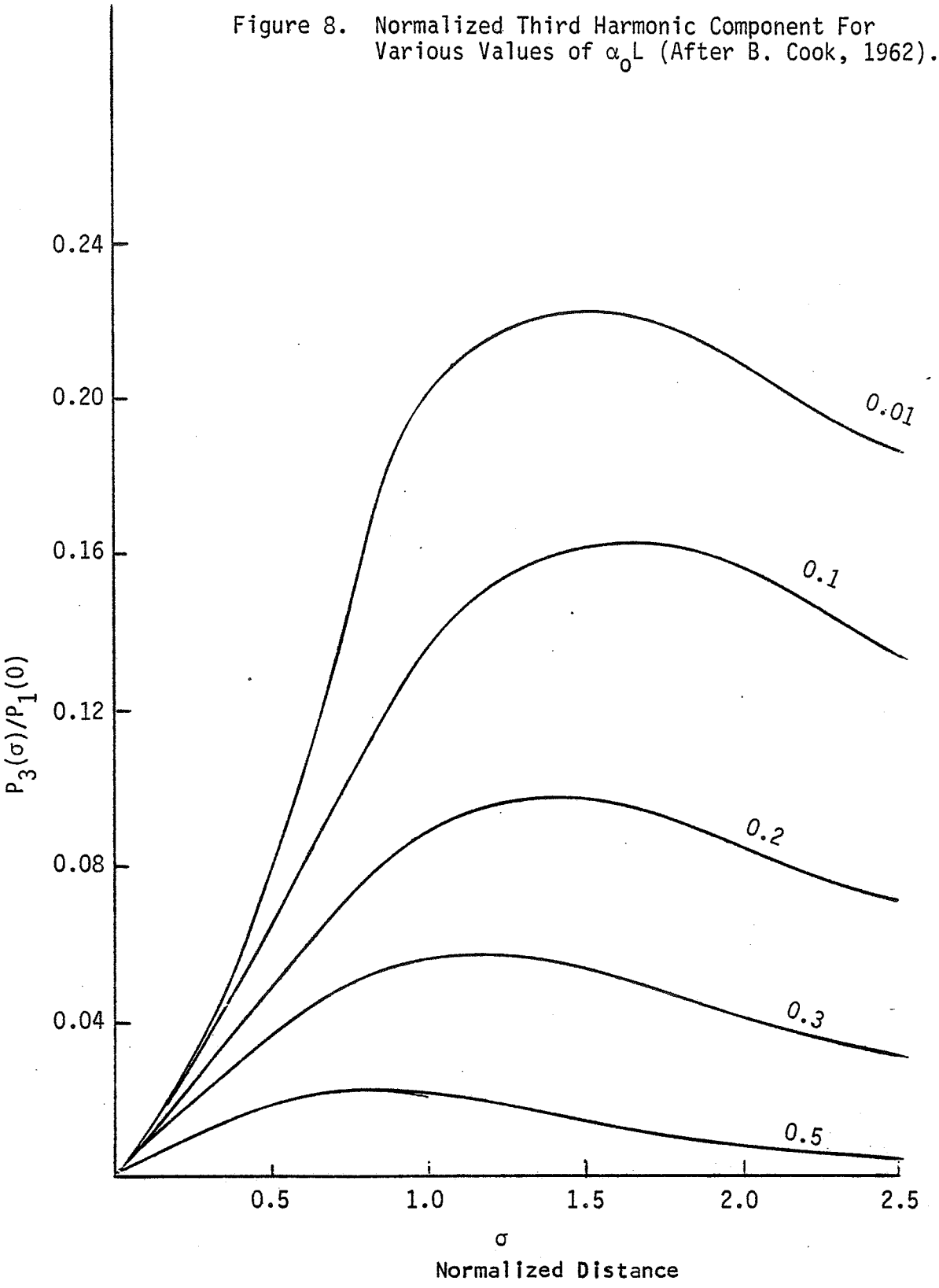

from source, and P is the acoustical pressure. The axial pressure exhibits a number of maxima and minima depending on the ratio a/λ.

Transverse to the axis, the beam pattern typically has a complex distribution with side lobes which change in number and magnitude at different points along the axis. At the last broad maximum around the near field/far field transition region, the transaxial beam pattern of the main lobe becomes a uniform Bell shape. Because the field is better defined in this region, many bio-ultrasound experiments have been performed in this region of the field. For this field, no simple complete theoretical description of finite amplitude waves yet exists. Therefore distortions in this region are frequently analyzed by assuming that the piston beam is a cylindrically collimated field of plane waves, for which the theory is well developed. However, the higher harmonics generated in the field of a piston source depend upon the three dimensional distribution of the fundamental frequency beam. It is not evident whether the harmonic components should greatly differ or closely resemble those predicted by a plane wave theory. The measurements performed in this project were intended to find an answer to this question for the special case, of a half inch diameter source at 3.2 MHz.

CHAPTER III: APPARATUS

The principle goal of the research was to measure the harmonic content of the signal generated by a piston source. A small diameter piezoelectric probe was used as a receiver. The output of the probe was fed to a spectrum analyzer, which determined the harmonic content of the received ultrasound wave. The probe was calibrated for sensitivity at harmonic frequemncies against a steel ball radiometer in a calibrating sound field of insignificant nonlinearity.

The block diagram of the measurement system is shown in Fig. 9. The tank in which the measurements were made was 22 cm long, 17 cm wide and 30 cm deep. A 25 cm column of castor oil at the end of the tank opposite to the source transducer was used as an absorber to reduce standing waves. All measurements were made in degassed water.

A Ferris model No. 22A variable frequency oscillator was used as the frequency source. The frequency of the oscillator was monitored by an HP 5314A frequency counter. To reduce the problem of reflections, the ultrasonic wave was pulse modulated by a pulsing unit constructed in this laboratory.

The pulsing unit was used to pulse modulate the signal from the oscillator to give RF pulses of different on and off times. In the manual mode, the same unit served as an on/off switch for continuous wave measurements. The pulsed signal was then fed to an Amplifier Research model AR-10LA broad band power amplifier. This unit was capable of providing up to 10 watts of RF electrical power, from 0.5

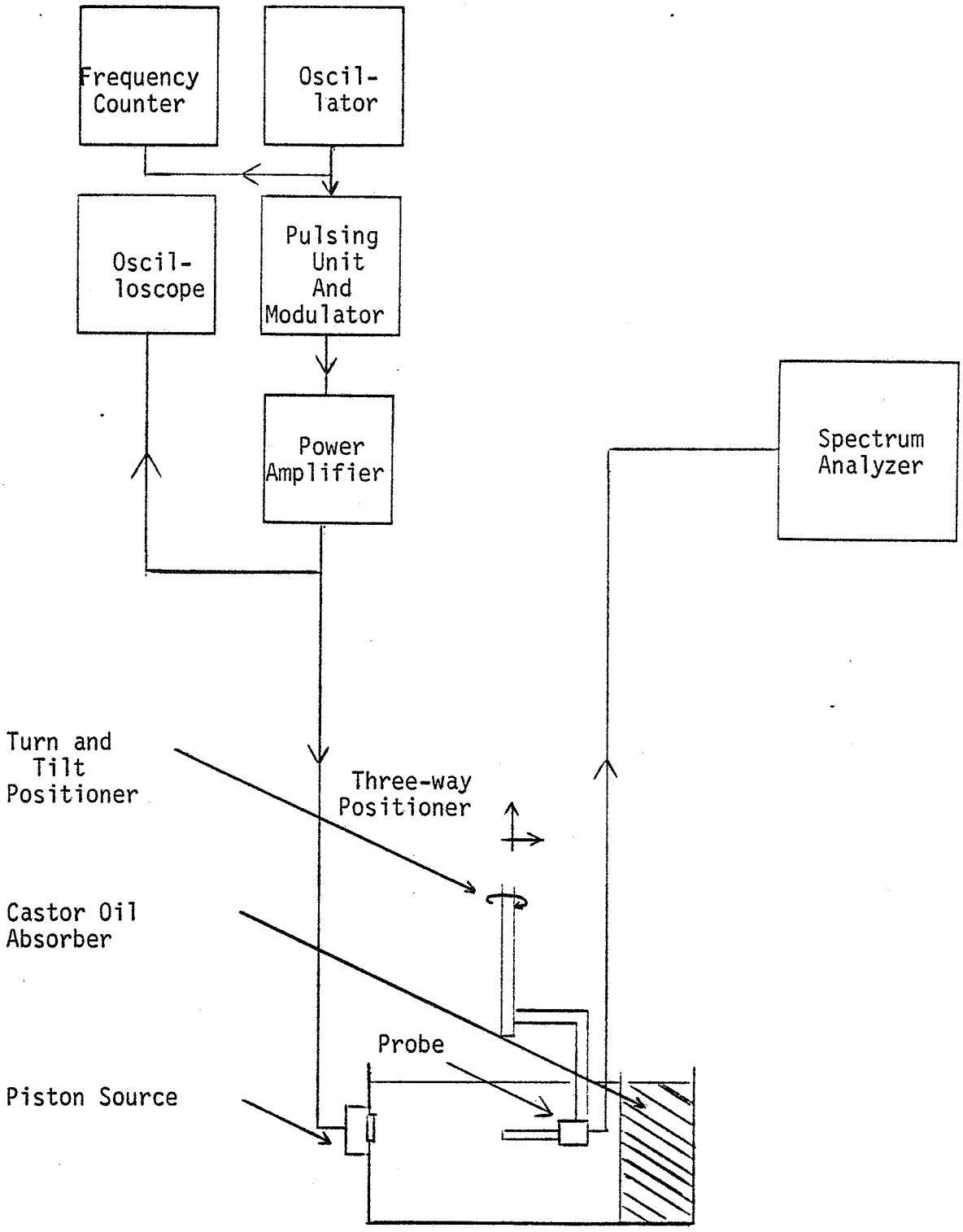

Figure 9. Block Diagram of Appartus

to 110 MHz. The RF signal was then fed to the ultrasonic transducer.

An HP model RM15 oscilloscope was connected across the transducer to monitor the voltage applied to the transducer and to ensure that the driving signal was not distorted. The source was excited in 50 μs pulses, one thousand times per second. Heating, standing waves, and echoes were thereby minimized, yet the pulses were long enough to ensure that continuous wave conditions existed in large portions of a pulse. As observed from piezoelectric probe measurements, the pulse amplitude stabilized in about 20 cycles.

The source transducers were half inch diameter, PZT4 Lead Zirconate Titanate ceramic transducers from Channel Industries (839 Ward Drive, P.O. Box 3680, Santa Barbara, CA 93105). These transducers were ceramic discs, with silver electrodes on both faces which served as the electrical terminals to the transducer. These discs were then mounted as shown in Fig. 10. A potting compound called Hysol was used to cement the transducer to its housing. Electrical connection to the ceramic disc was provided by gold foils about 2 mm wide and 0.25 thick. Silver paint from G. C. Electronics was used as conductive cement to make the electrical connection between the gold foil and the transducer terminals. The D.C. resistance of the electrical connections described above was measured to be less than 0.1 ohm.

Three different frequencies--3, 6 and 9 MHz, were needed in this study and were provided by two ½ inch diameter transducers. A 3MHz transducer working at its fundamental and third harmonic provided ultrasound frequencies of 3.23 and 10.04 MHz. A ½ inch diameter, 2 MHz

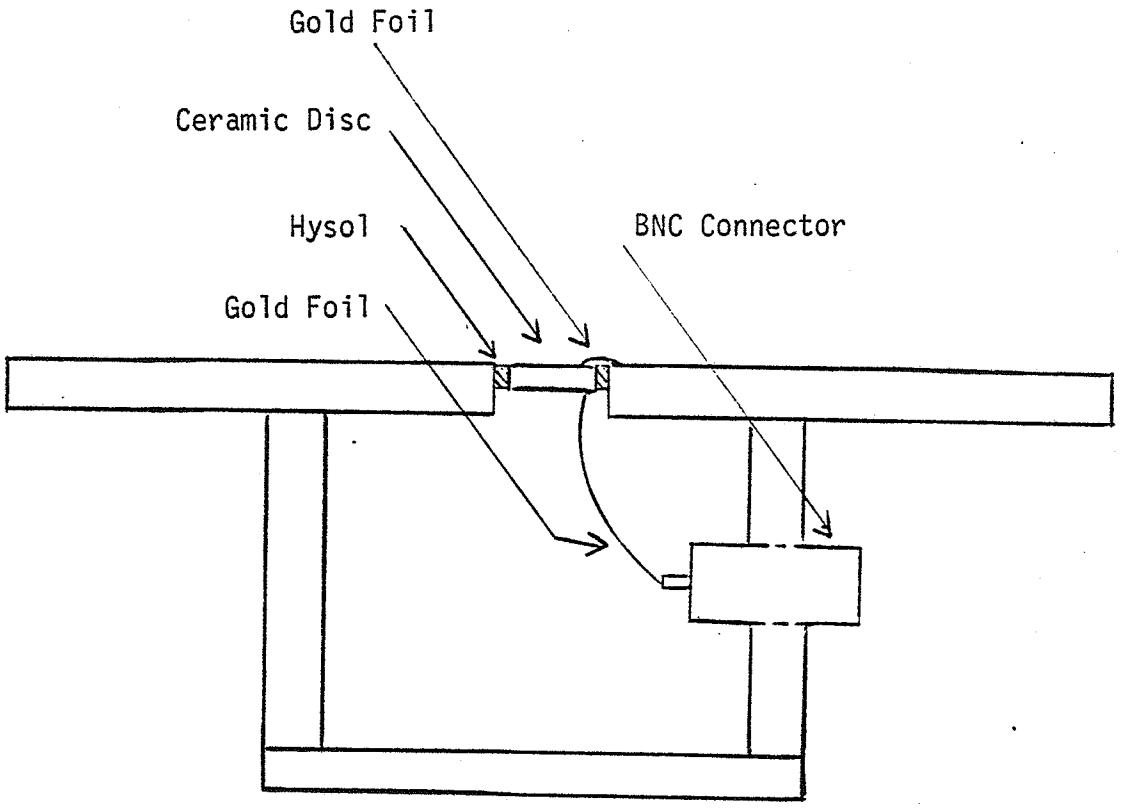

Figure 10. Source Transducer Housing and Mounting.

transducer working at its third harmonic resonance provided signals at 6.81 MHz. In order to provide broad sound beams in some of the calibration procedures, these transducers were equipped with a detachable stainless steel aperture 1/8 inch in diameter.

A 2 mm diameter PZT4 ceramic disc from Valpey Fisher Corporation (Holliston, Massachusetts) was used as a receiving element. The resonant frequency of this disc was around 20 MHz in the thickness mode. The detailed construction of the hydrophone probe is shown in Fig. 11. The ceramic disc was cemented with silver paint to the end of a copper rod 5 cm in length and 2 mm in diameter. The rod was then slipped into a nylon insulating sleeve which fit the rod snugly. The rod and sleeve was in turn slipped into a stainless steel tube 3 mm in outside diameter. Epoxy adhesive was then applied with a syringe and needle to seal off the space between the ceramic disc and the stainless steel tubing. The outside face of the ceramic disc was then electrically connected to the stainless steel tubing with silver paint.

The tube and the copper rod were finally connected, respectively, to the ground and central conductor of a 50 Ω RG 174 coaxial cable. The cable length was 1.5 feet and was connected directly to an HP 85 - 52A Spectrum Analyzer. Because the piezoelectric receiver (hydrophone) is a phase sensitive device, it was important to adjust it so that the receiving element was parallel with the source transducer. The hydrophone was therefore mounted on a turn and tilt positioner, which allowed rotation in two orthogonal planes. The entire setup was then mounted on an X Y Z positioner for placement of the hydrophone.

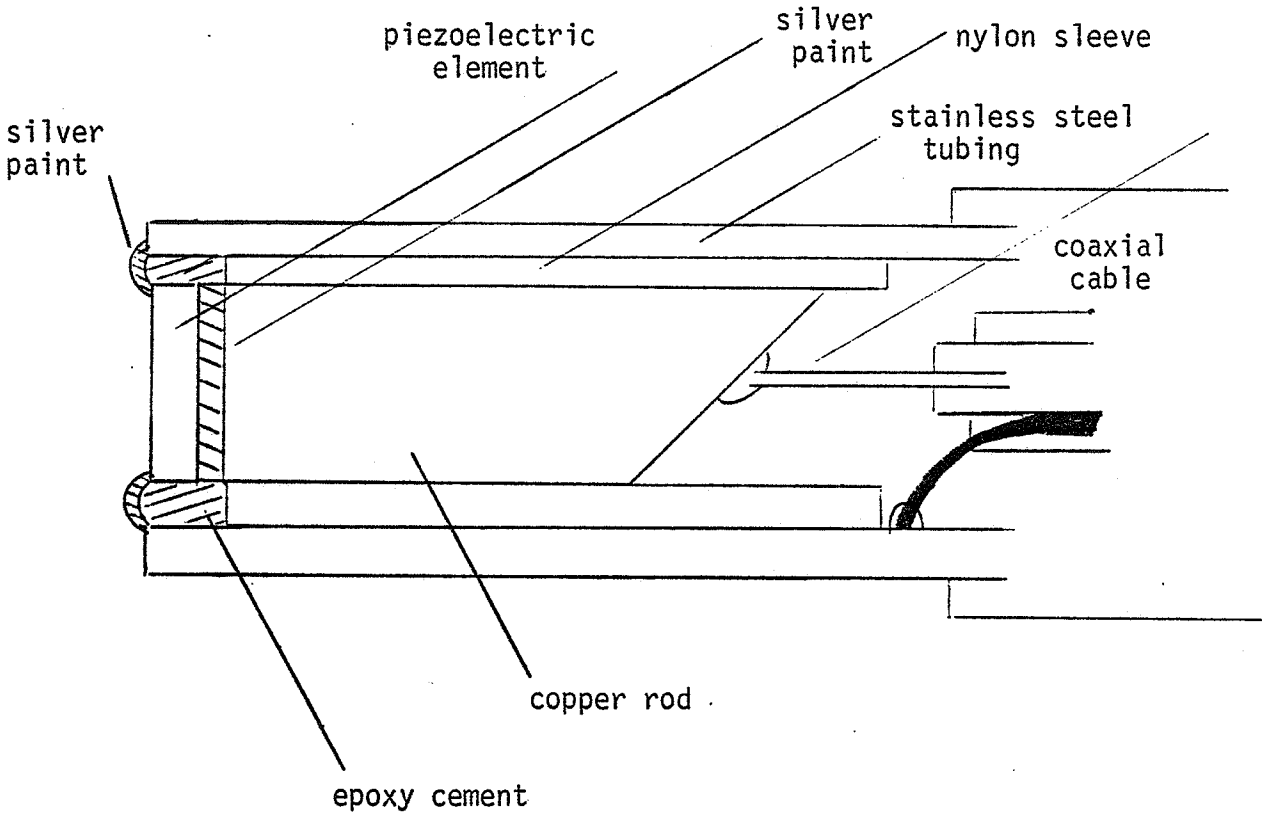

Figure 11. Hydrophone Construction

CHAPTER IV: CALIBRATION

A. Source

Due to diffraction, the intensity distribution near a piston source is very complex. Therefore no attempt was made to measure the intensity distribution at the source. Instead, the average source intensity was measured. The average source intensity was defined as

$$I_{av} = \frac{\text{Total acoustical power output from the source}}{\text{Effective area of source}}$$

To obtain the total acoustical power, the radiation force on an absorber which intercepted the entire beam was measured. The arrangement for measurement is shown in Fig. 12. The absorber was a rectangular block of soab rubber, 4 cm by 4 cm in area and 3 cm thick. The rubber target was suspended with surgical silk in the shape of an inverted "V". The radiation force was determined by measuring the deflection of the rubber target and solving the force triangle, which gives $F_r = mgd/l$ for small d. Here, F_r is the radiation force, m is the weight of the target in water, g is the gravitational acceleration, d is the horizontal deflection of the target, and l is the effective length of the pendulum system. Since the force per unit area on an absorbing target, i.e. the radiation pressure P_r is given as $P_r = I/c_o$ where c_o is the small amplitude phase velocity, and I is the incident intensity, the total acoustical power W, which is the integration of intensity over the beam, is related to the radiation force by the expression $W = \int I ds = \int c_o P_r ds = c_o F_r$, where s is the area of the beam.

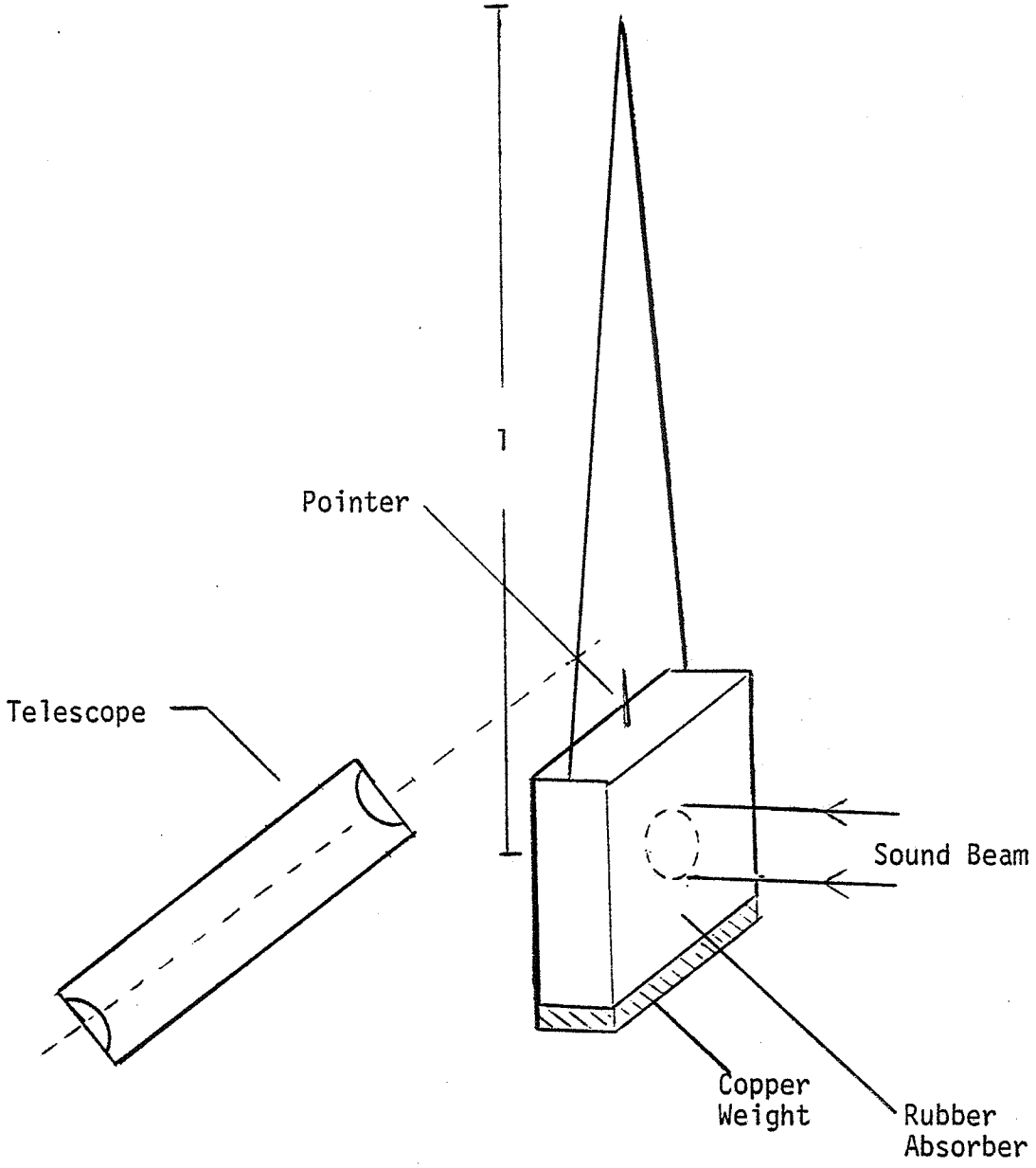

Figure 12. System for Total Power Measurement. Includes a Suspended Absorbing Target and Optical Telescope to Measure Displacement.

The intensity reflection coefficient of sound at the water and rubber interface was estimated by a pulse echo method to be around 0.03. The assumption of a totally absorbing target was therefore valid.

The absorbing target was then placed at 3 cm from the source to measure the total acoustical power. At this distance, nonlinear losses in the medium are negligible. A plot of the measured total acoustical power vs. the square of drive voltage of the 3.2 MHz source is given in Fig. 13. As seen from the plot, the source transducer had negligible nonlinearity up to at least 5.7 watts of acoustical output. For some aspects of this study, a knowledge of source pressure was needed. It was estimated as $P_{o\,av}^2 = \rho_o c_o I_{oav}$.

B. Hydrophone

The sensitivity of the hydrophone at the first three harmonic frequencies of the 3.2 MHz source was obtained by comparison with the steel ball radiometer at intensities low enough so that the nonlinearity of the medium was negligible. The steel ball radiometer consisted of a type 440c stainless steel sphere, 1.6 mm in diameter, that was suspended by a nylon monofilament in a bifilar suspension. For this arrangement, the intensity is related to the radiation force F_r on the sphere through the expression (Dunn et al., 1977) $I = F_r c_o/\pi a^2 Y$, where a is the radius of the sphere, Y is the acoustic radiation force function described below and c_o is the infinitesimal amplitude wave velocity. Here F_r was again obtained by observing the deflection of the pendulum system and solving the force triangle, so

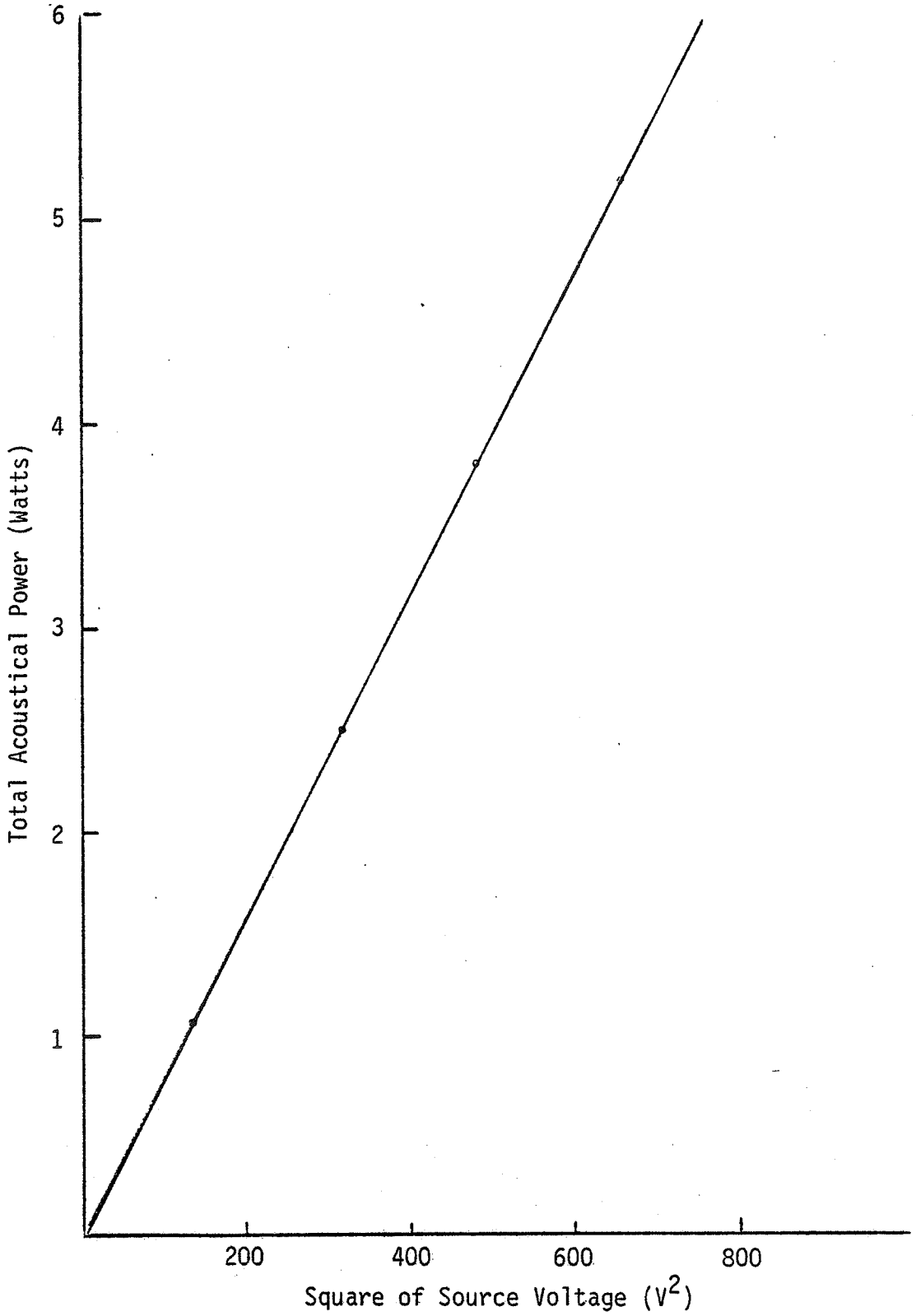

Figure 13. Total Acoustical Power vs. Square of Source Voltage at 3 cm From Source.

that F_r = mgd/l, for small deflection d.

The "Y" parameter is a function of Ka, where K is the propagation constant and a is the radius of the sphere. The sensitivity of the steel ball is therefore a function of both frequency and ball size. The "Y" value for the steel sphere used has been calculated by Hasegawa (Hasegawa, 1969) and has been verified experimentally by Dunn et al. (Dunn, 1977). The Ka and Y values for the steel ball of this study at frequencies of interest are listed in Table 1.

TABLE 1

Ka and Y Values For Frequencies Used In Calibration

f	Ka	Y
3.23 Mhz	10.14	.79
6.87 MHz	22.84	.88
10.06 MHz	33.45	.92

At the frequencies of calibration, streaming may have a significant effect on the ball deflection. An acoustical window was therefore placed in front of the steel ball to reduce this form of interference.

The calibration of the receiver had to be accomplished in a linear acoustic field in order to make possible the measurement of nonlinear effects. This required using small source intensities and

working as close to the source as possible. However, to provide a uniform yet broad enough calibration field, one must work beyond the near field distance of the source, which is given approximately by $d = a^2/\lambda$, where a is the radius of the source and λ is the wavelength of sound in the medium. It was found that due to finite amplitude effects, a half inch diameter source at 6.81 and 10.06 MHz could not generate such a field without appreciable distortion.

The problem was dealt with by reducing the effective diameter of the source. A ¼" thich steel plate with a 1/8" diameter hole was placed in front of the source, thus reducing the effective source aperture to about 1/8" diameter. The transaxial beam pattern of these sources with reduced aperture is plotted in Fig. 14, normalized to have the same peak value. Measurements were made at 12 cm from the source for 3 and 6 MHz, and 8 cm from the source for 10 MHz. To ensure that these calibration fields had negligible nonlinearity at calibrating levels, the pressure magnitudes at the calibration position were measured for several source voltages. The measured pressure values are shown in Fig. 15 against source voltages. The deviation from linearity at the calibration levels was found to be less than 3%.

The techniques described above were used to calibrate the hydrophone, and the figures of sensitivity are given in Table 2. The steel ball radiometer determination of intensity is accurate to within ±10%. The uncertainty in pressure magnitude due to averaging of the bell shaped calibration beam over the area of the hydrophone probe was about 5% for 3.23 MHz, 10% for 6.87 MHz, and 20% for 10.06 MHz.

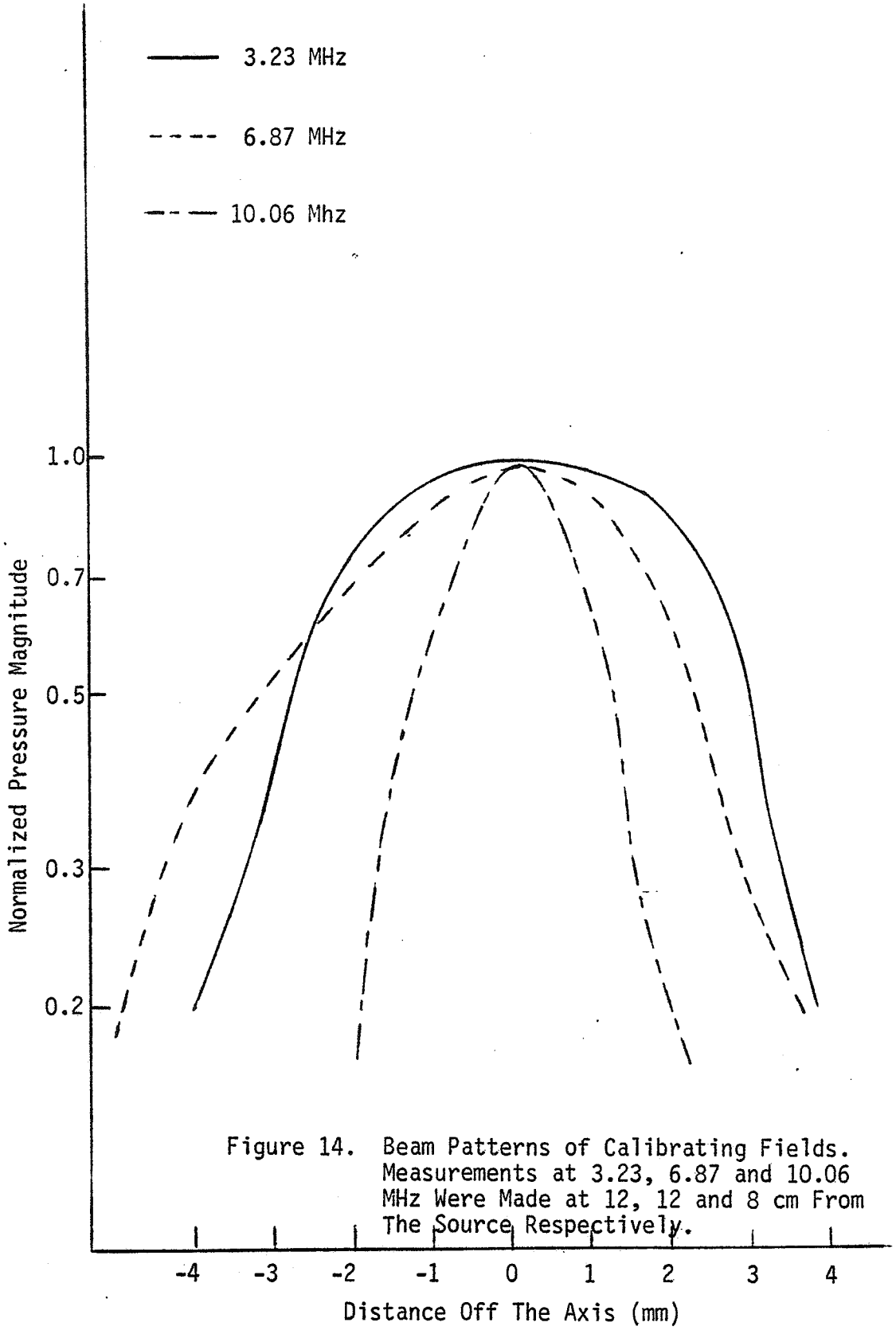

Figure 14. Beam Patterns of Calibrating Fields. Measurements at 3.23, 6.87 and 10.06 MHz Were Made at 12, 12 and 8 cm From The Source Respectively.

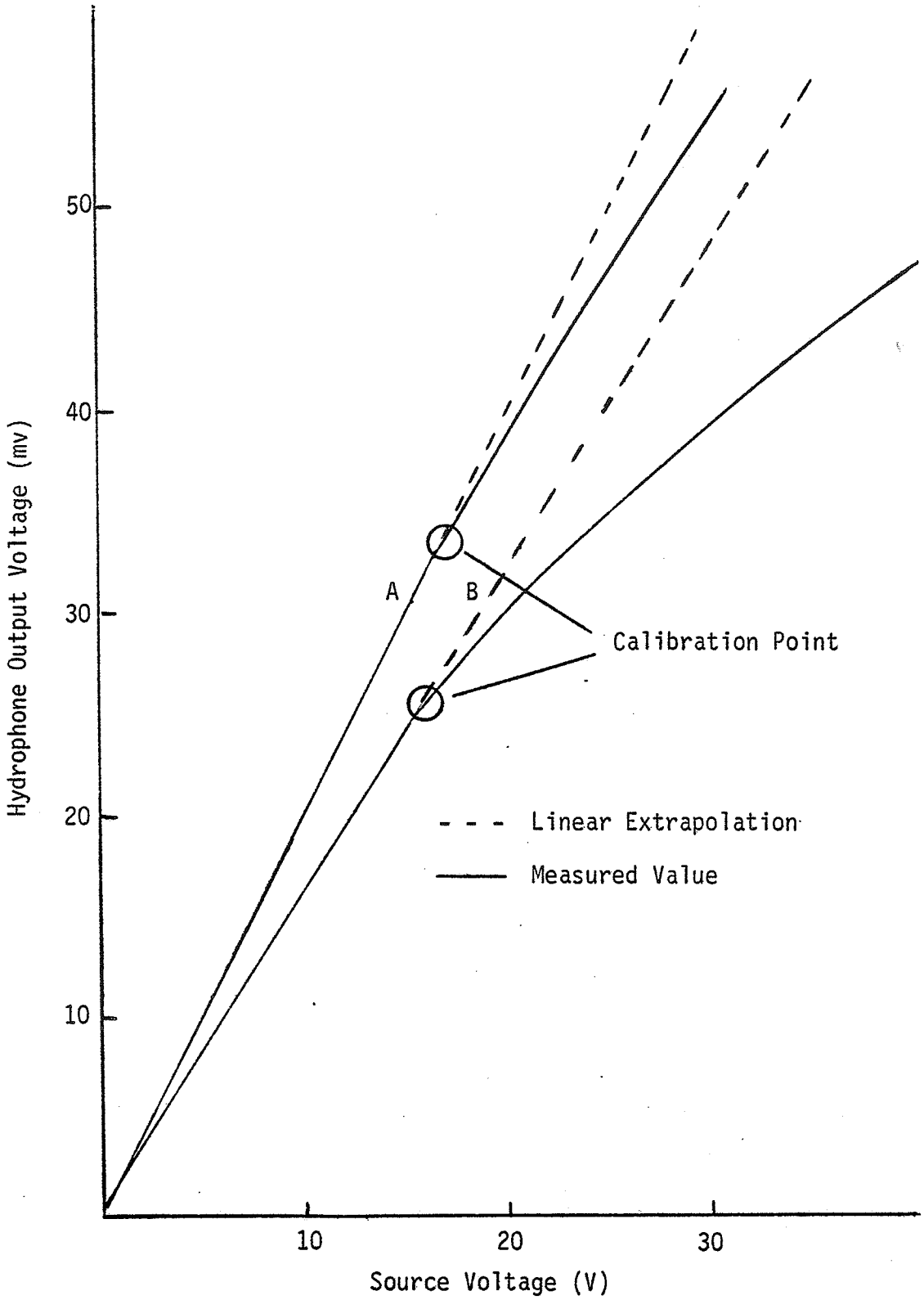

Figure 15. Hydrophone Output Voltage vs. Source Voltage At Calibrated Position. Curve A is 6.87 MHz at 12 cm From The Source; Curve B is 10.06 MHz at 8 cm From The Source

These estimated maximum errors are also listed in Table 2. Since the same field was used for steel ball deflection measurement of intensity, and the steel ball was of similar size as the hydrophone, the "averaging" errors may in part cancel each other during the calibration process.

TABLE 2

Hydrophone Sensitivity And Error Margin

Frequency	Sensitivity (V/P)	Maximum Error
3.23 MHz	.017 volt/atm.	15%
6.87 MHz	.030 volt/amp.	20%
10.06 MHz	.039 volt/amp.	30%

C. Linearity of Transmitting-Receiving System

The linearity of the source transducer was illustrated by the total acoustical power measurement mentioned in the section on source calibration. The total acoustical power was found to be linearly dependent upon the square of source voltage up to at least 5.7 acoustical watts.

Linearity of the complete measuring system including the transmitter and receiver was further checked by observing the output of the hydrophone at a distance of 2 cm from the source. At this distance,

the magnitude of the received fundamental component followed the drive voltage linearly up to the point of maximum drive, about 27 volts rms across the transducer. This drive level produced about 5.7 watts acoustical power, and a local pressure of six atmospheres at one of the near field maximum at which the hydrophone was placed. The magnitude of the harmonics was found to be always less than 5% of the fundamental throughout the range of measurement. The entire measurement system was therefore believed to be approximately linear up to the drive level stated above.

D. Effective Area of Source

The effective area of the piston source is approximated in this study to be the same as the surface area of the source. However, due to edge effects, this may not be an accurate estimation. It was observed that at some point along the axis of the piston source, the measured axial pressure reaches 2.7 times that of the estimated average source pressure. This contradicted the results of the plane piston theory which predicts a maximum increase of a factor of 2. An investigation of the effective area of the source is now in progress.

E. Reliability Of Hydrophone Measurements

The reliability of the hydrophone measurements is discussed separately in the Appendix.

CHAPTER V: DATA AND DISCUSSION

Previous discussion in Chapter 2 indicated that the pressure distribution in the near field of a piston source is very complex and that no satisfactory theory yet exists to predict the behavior of finite amplitude waves in this region. In the absence of an applicable theory, the approximate picture is often used--that the sound beam from a piston source is a collimated plane wave up to approximately a^2/λ from the source, and within this region, the acoustic pressure magnitude is essentially uniform with distance.

However, the actual field, especially along the axis of the piston, departs markedly from a constant value. The pressure amplitude fluctuates widely near the source, and in the vicinity of the last broad maximum the axial pressure increases substantially. In this region, a large portion of the energy in the beam is concentrated in an area much smaller than the area of the piston source, a phenomenon which is called "self focusing" by some researchers (Zemanek, 1971). The word "focusing" here and throughout the discussion is used loosely to refer to the concentration of energy due to diffraction.

Considering the above mentioned facts about a piston source, the plane wave approximation at its best has the character of an averaging effect, and in some cases, depending on the value of a/λ and the distance from the source, may be totally inaccurate. To provide some insight into the problem, this section reports on the measurement of harmonic content in the field generated by a 3.23 MHz, ½" diameter piston source. Three cases were investigated.

Case I. Axial Behavior

A. A fixed source level at 3.1 atm (3.3 W/cm^2), variable distance.

Figure 16 shows the values of the pressure amplitude along the axis at an average source pressure of 3.1 atm (3.3 W/cm^2). It was observed that starting at 3 cm from the source, the amplitude of the first harmonic (i.e. the fundamental) rises continuously until it reaches a peak value of 8.5 atm at 7 cm from the source. The acoustic pressure then begins to decrease, but at a slower rate, as the probe is moved further away from the source. Thus for this particular transducer, the axial pressure at some points can be as much as 2.7 times greater than the estimated source pressure, i.e. an increase in intensity by a factor of 7.

The second and third harmonics exhibit a rapid increase in magnitude with distance. Going from 3 cm to 6 cm from the source, the second harmonic magnitude increased by almost tenfold. A plane wave theory would predict the second harmonic magnitude to increase with $P_1^2(0)$ x, i.e. going from 3 cm to 6 cm, the second harmonic magnitude should be about doubled. Obviously, the measured second harmonic magnitude is increasing at a much faster spatial rate than that predicted by a plane wave theory.

The increase can be explained qualitatively by a "self focusing" model, applicable to the point of near field/far transition. The hypothesis is that: a) The fundamental and higher harmonic energy is

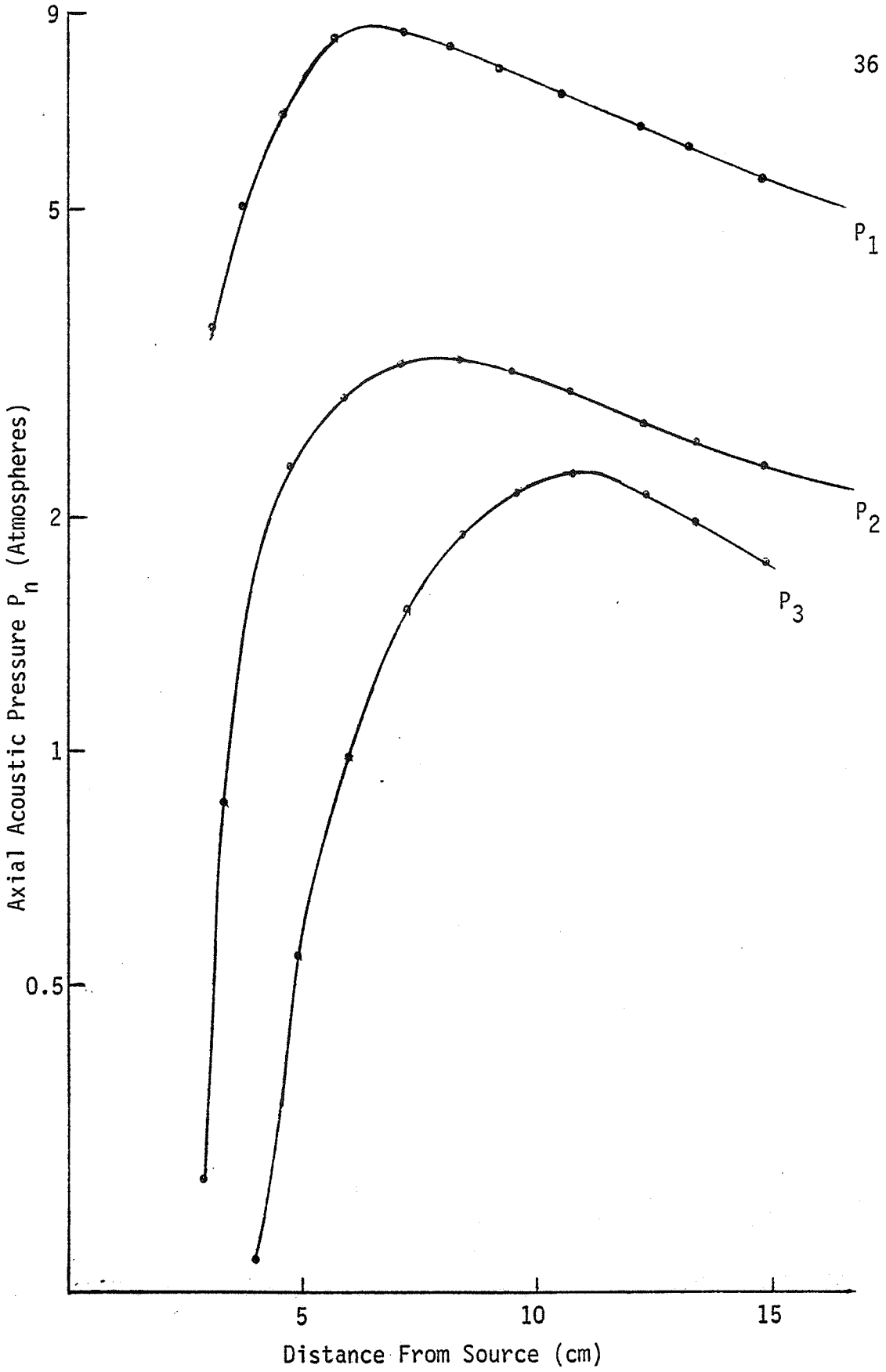

Figure 16. Harmonic Pressure Magnitude At Different Distances From Source.

concentrated into consecutively smaller areas as the wave moves away from the source, resulting in higher acoustical pressure values for both. b) The generation of higher harmonics is increased due to the increase in the magnitude of the fundamental hypothesized in a).

Since the fundamental magnitude changes with distance, a more meaningful way to express the harmonic content would be to use the relative harmonic magnitude P_n/P_1, where P_n is the magnitude of the nth harmonic, and P_1 is the magnitude of the fundamental at the same distance. Figure 17 is a plot of P_n/P_1 as a function of distance from the source.

It is perhaps interesting to note that at distances between 11 and 15 cm, the ratios of the second and third harmonic magnitudes to the magnitude of the fundamental reach a maximum of one half and one third, respectively, which is expected for a sawtooth wave. From the plane wave finite amplitude theory, this occurs around $\sigma = 3$, i.e. at three times the discontinuity distance. With the source pressure used in the measurement, $\sigma = 3$ corresponds to a distance 45 cm from the source. If a plane finite amplitude wave were to generate the above mentioned amount of distortion at 15 cm from the source, a source pressure of 9 atm (three times higher than the source pressure used) would be required. The previous observation that the fundamental magnitude increases by a factor of three along the axis agrees approximately with this figure.

B. Fixed distance at 12 cm from source, variable source level.

Discussions in the theory section indicated that the finite

Figure 17. Relative Harmonic Content Along Axis.

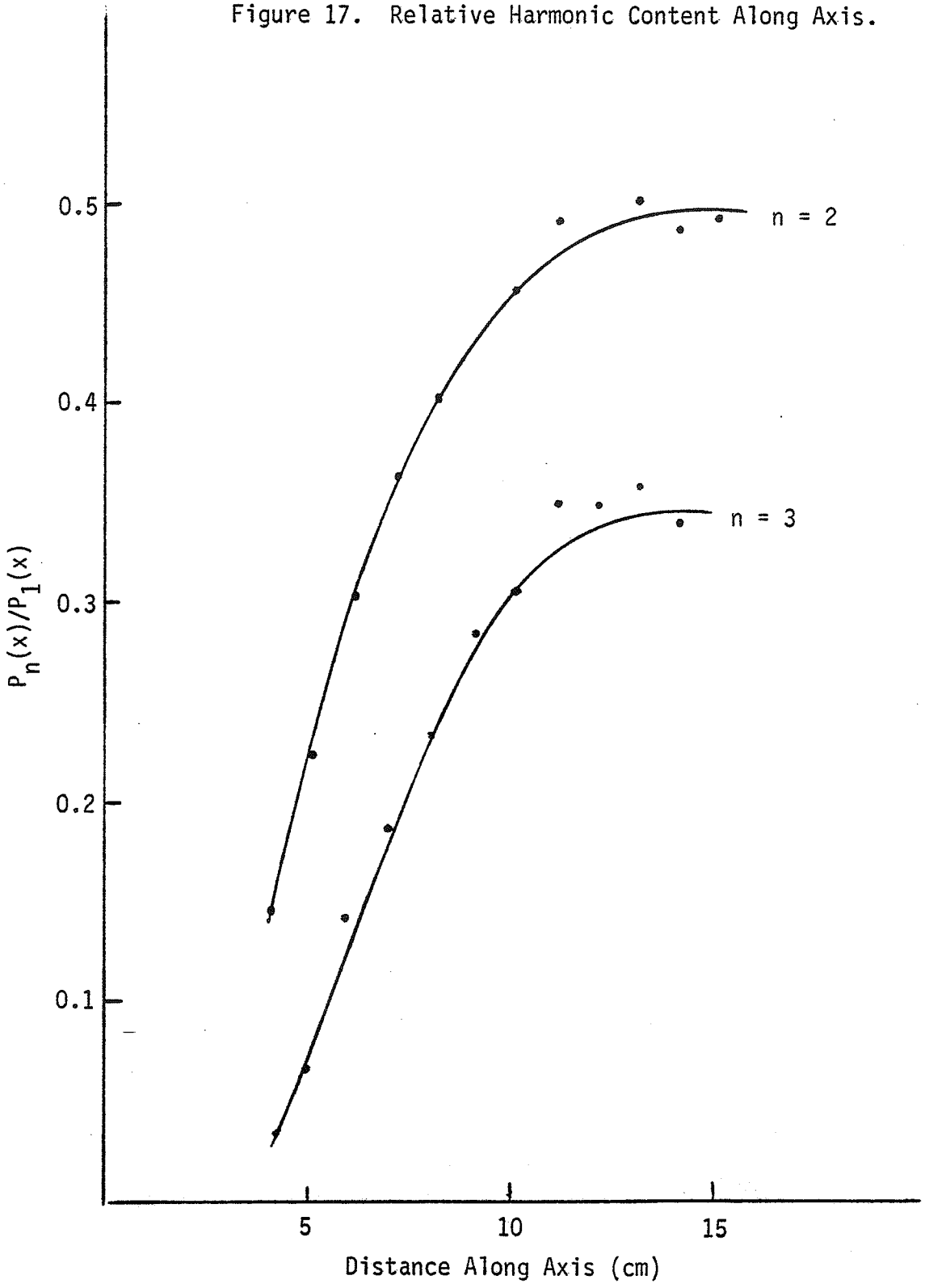

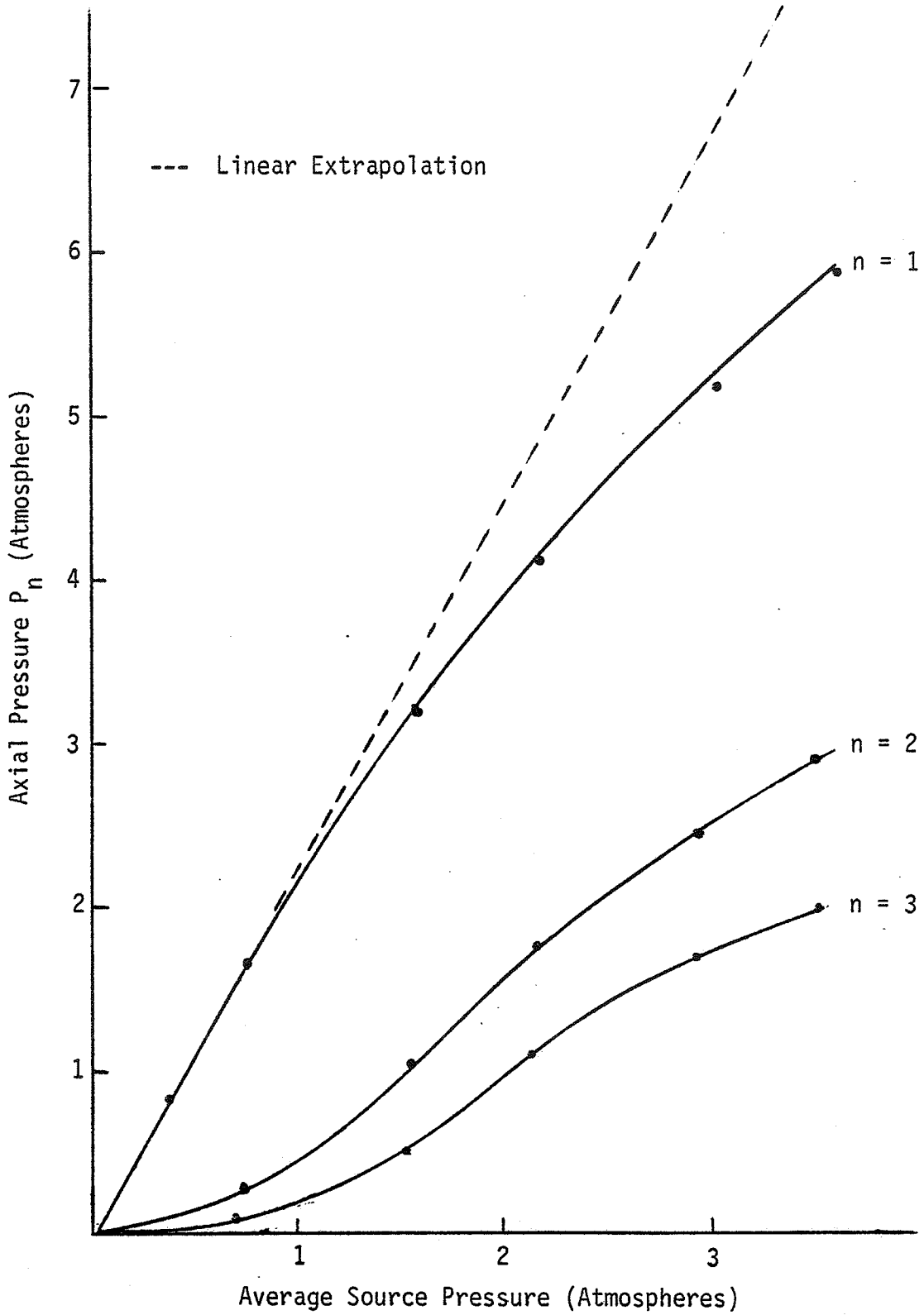

Figure 18. Axial Pressure vs. Average Source Pressure Measured At 12 cm From Source For The Fundamental, Second And Third Harmonics.

Figure 19. Deviation Of Fundamental Magnitude From Linearity At Different Source Pressures.

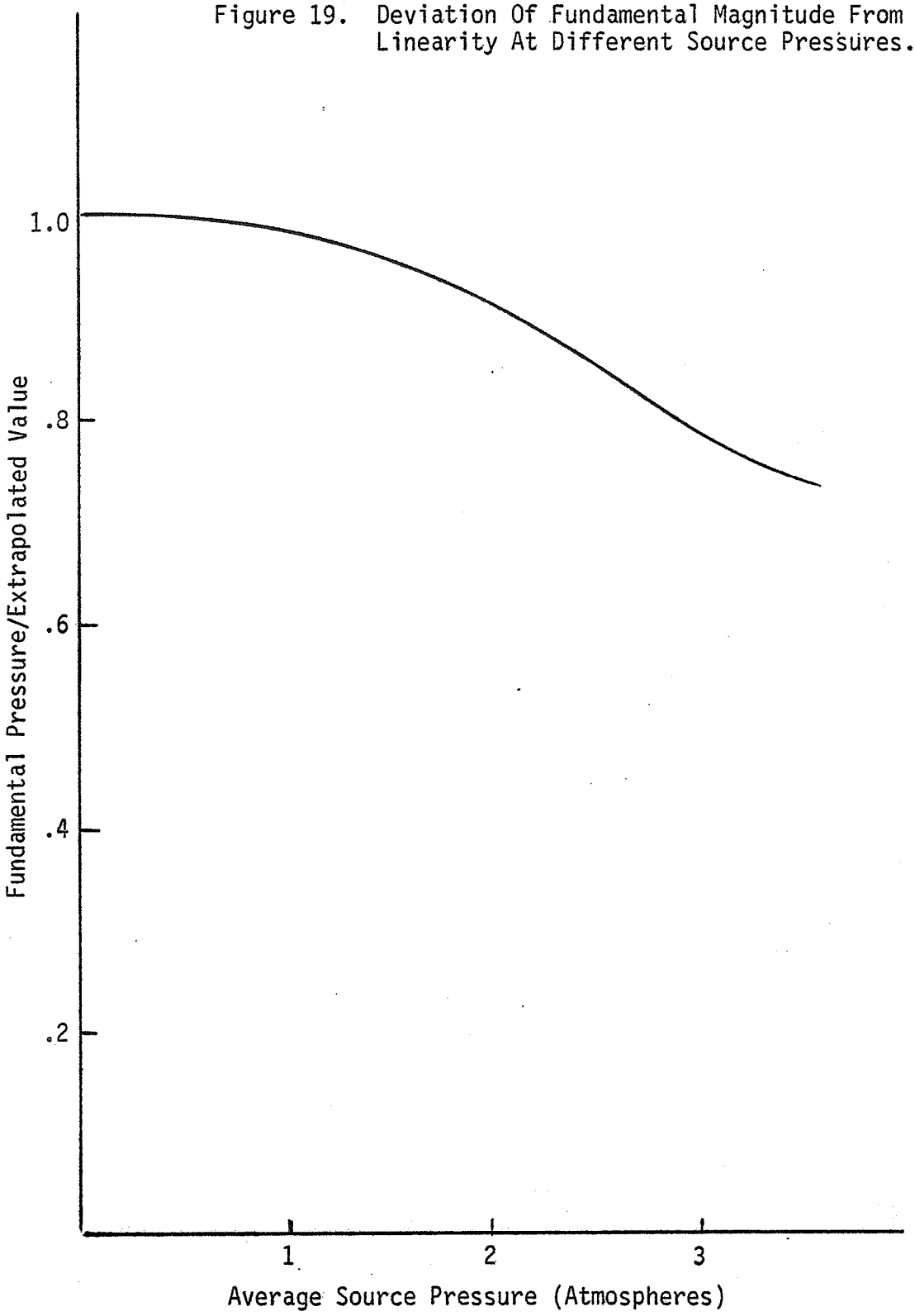

Figure 20. Relative Harmonic Magnitude vs. Average Source Pressure.

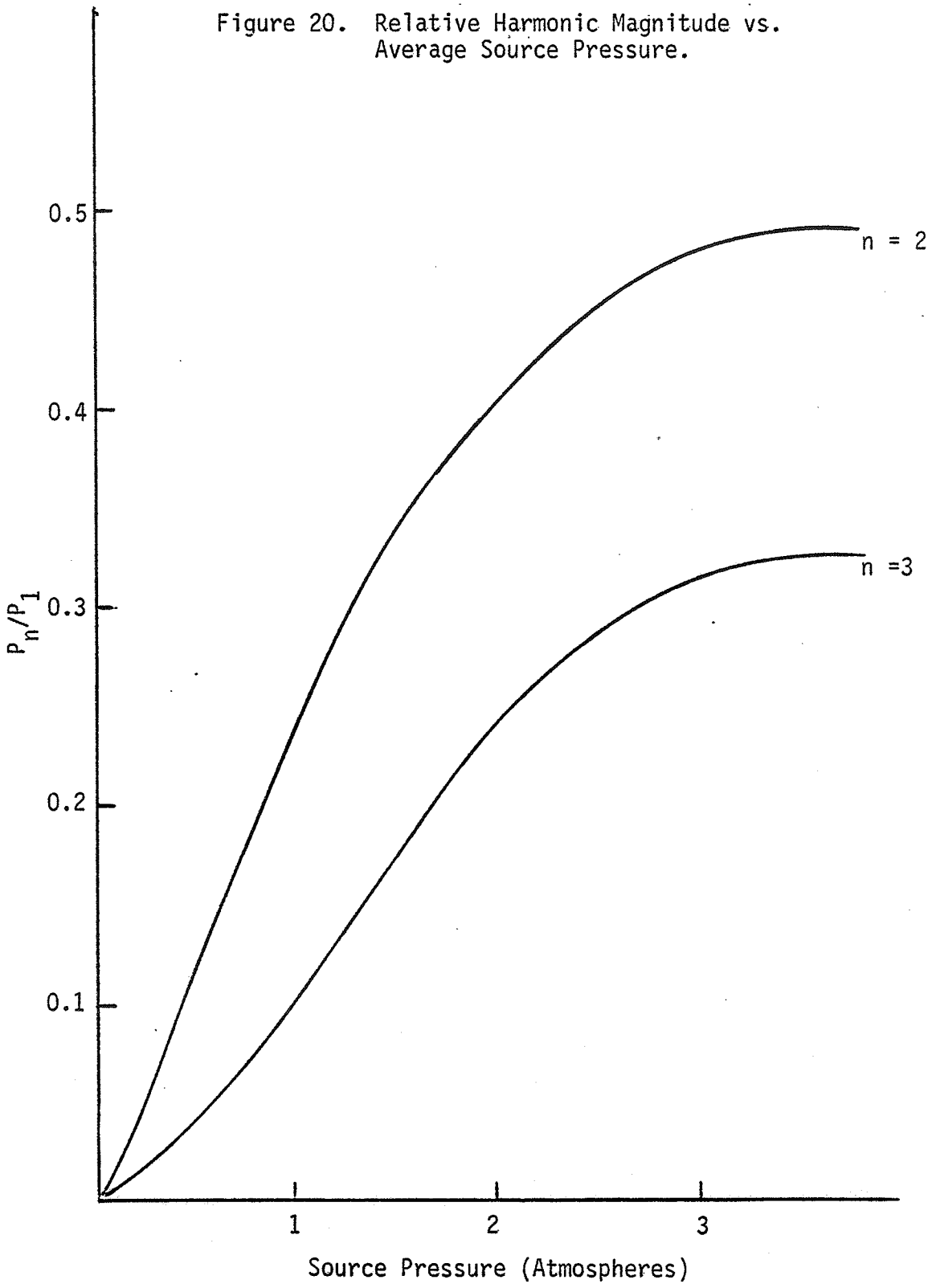

Figure 21. Beam Patterns Of Fundamental And Harmonics At Source Pressure Of 1.56 atm Measured At 12 cm From Source.

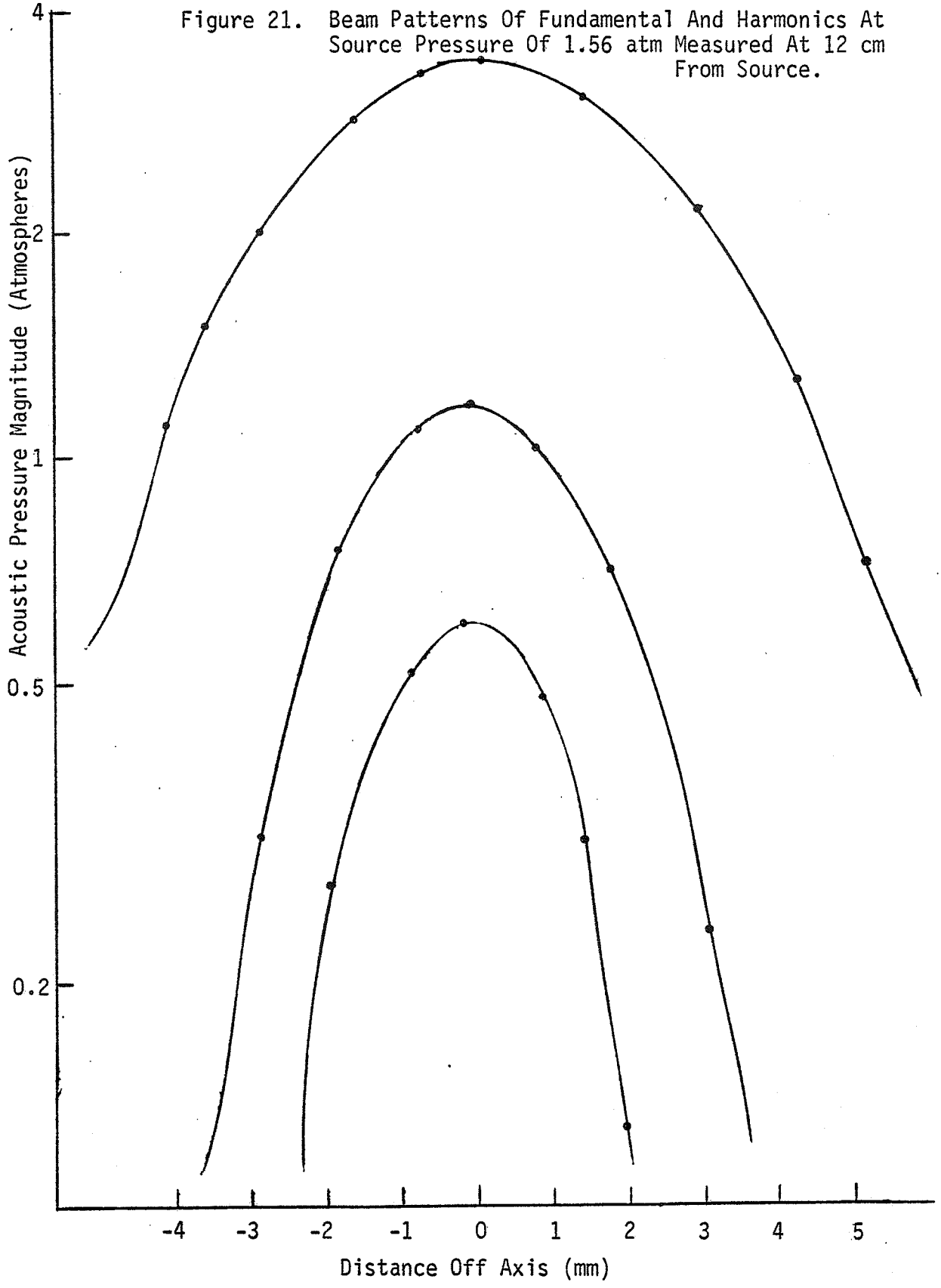

at a source pressure of 1.56 atm. The pressure distributions showed the expected bell-shaped amplitude variation across the axis, with minor lobes at larger distnaces from the axis. These beam profiles were approximately symmetrical around the main axis. It was observed that the beam widths of the higher harmonics were smaller than the fundamental, so that the relative harmonic magnitude P_n/P_1 was highest on axis, and decreased as the probe was moved off axis.

This observation may be explained as follows: At the near field/far field transition region, the magnitude of the fundamental is highest on axis and decreases on points off axis. Since the second and third harmonic magnitudes are proportional respectively to P_1^2 and P_1^3 (Eq. 6, 7), it is expected that transverse to the axis the higher harmonics will change at a faster spatial rate than the fundamental, resulting in a beam profile sharper than that of the fundamental. Lockwood et al. (Lookwood et al., 1973) reported a similar sharpening of the beam profile with harmonic number at the far field of a piston source. According to their analysis, if the directivity function of the fundamental is $D(\theta)$, and the distance from the sources is much less than the discontinuity distance, the directivity function of the nth harmonic would be $D^n(\theta)$. However, at the near field of a piston source, the equation is not expected to be applicable.

It was further observed that the beam widths of the three harmonic components broaden with increasing source level. Figure 22 is an illustrative plot of beam patterns for high and low source pressures, normalized to have the same peak values for easy comparison.

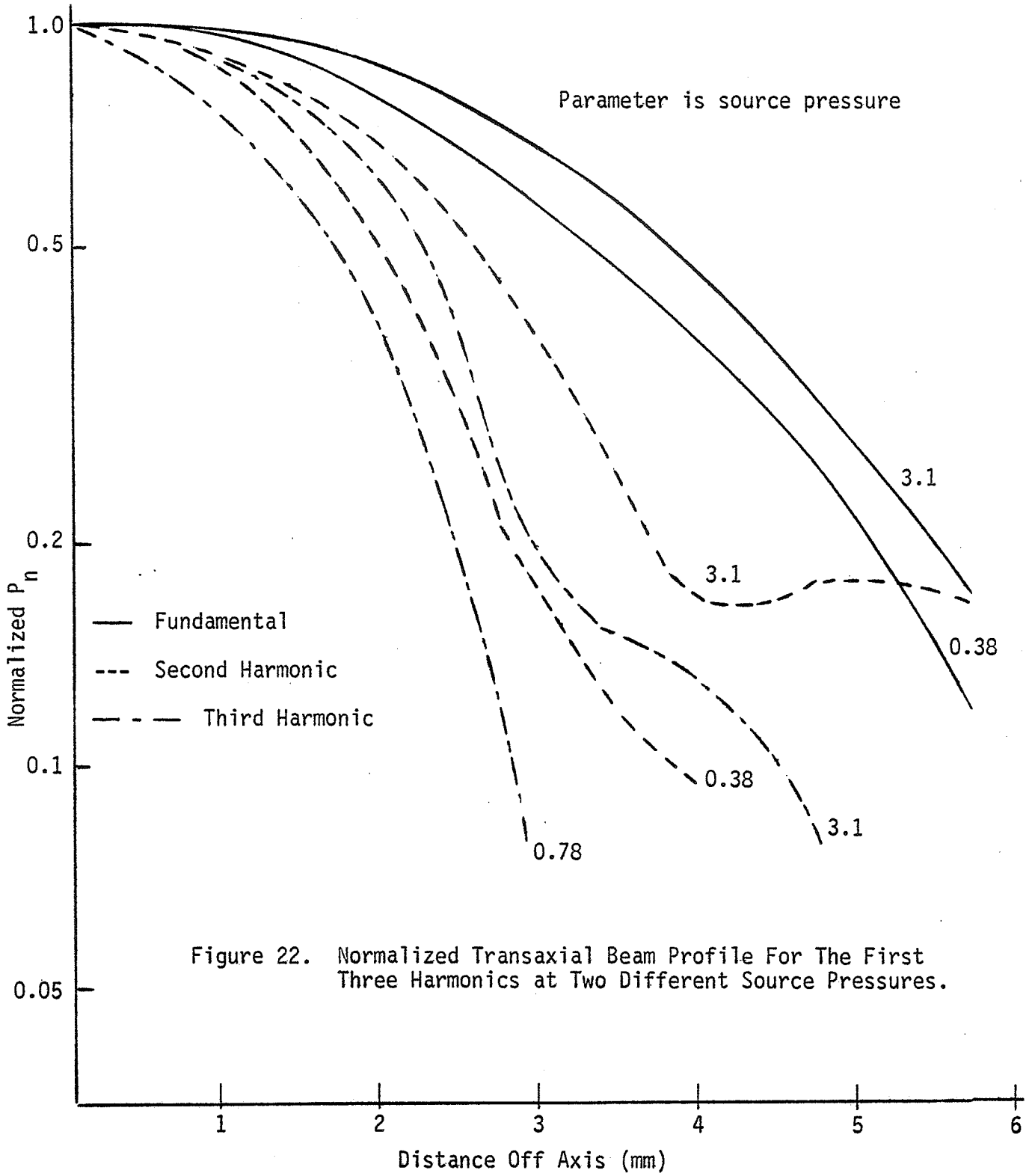

Figure 22. Normalized Transaxial Beam Profile For The First Three Harmonics at Two Different Source Pressures.

The half power beam width of the fundamental is widest, about 4.6 mm for a source pressure of .38 atm, increasing to 5.5 mm at a source pressure of 3.1 atm, a factor of 1.2 increase. The second harmonic is about 3.2 mm wide at a source pressure of .38 atm, increasing to 4 mm at a source pressure of 3.1 atm, a factor of 1.3 increase. The third harmonic is about 2.3 mm wide at a source of .78 atm, increasing to 3.7 mm for a source pressure of 3.1 atm, a factor of 1.6 increase. Table III is a list of the half power beam width for the three harmonics at various source levels.

TABLE 3

Half Power Beam Width (mm) For The Three Harmonics At Different Source Pressures. f_1 = 3.23 MHz f_2 = 6.87 MHz f_3 = 9.69 MHz

	P_{oav}(atm)				
	.31	.78	1.56	2.18	3.10
Beam width for f_1	4.4	4.6	4.8	5.0	5.5
Beam width for f_2	3.2	3.2	3.0	3.4	4.0
Beam width for f_3	---	2.3	2.5	2.7	3.7

The broadening of the fundamental beam profile is probably a result of the extra attenuation (transfer of energy to higher harmonics) caused by nonlinear effects. The more intense part of the beam suffers

greater attenuation than the off axis portions, so that the beam pattern appears more blunt than for the small amplitude case. The broadening of the higher harmonic beam profiles is probably a result of saturation. The amplitude of the higher harmonics cannot exceed that of a sawtooth wave, i.e. P_n/P_1 has a maximum value of 1/n. When the axial harmonic magnitude approaches this limitation, the growth rate with source pressure tends to slow down. The harmonics in the off axis portions of the beam then grow at a faster rate relative to those in the on axial portion, resulting in a broader beam profile.

Case III. Spatial Average Harmonic Content

The fact that beam widths of the higher harmonics are smaller than the fundamental showed that the harmonic energies are more concentrated around the axis. As a result, the spatially averaged value of the harmonics should be smaller than the axial value. Since the hydrophone responds to pressure rather than intensity, we define a quantity called spatially averaged pressure. It is obtained by integrating the pressure magnitude over an area equal to the effective area of the source, and then dividing the integral by the source area. This quantity will represent that measured when the entire beam is intercepted by a pressure sensitive device, such as a large size piezoelectric receiver.

Figure 23 shows the spatially averaged pressure of the three harmonics at different source pressures. If Fig. 23 was compared with the axial plot on Fig. 18, one observes that the averaged pressure is generally lower in magnitude than the corresponding axial value, as

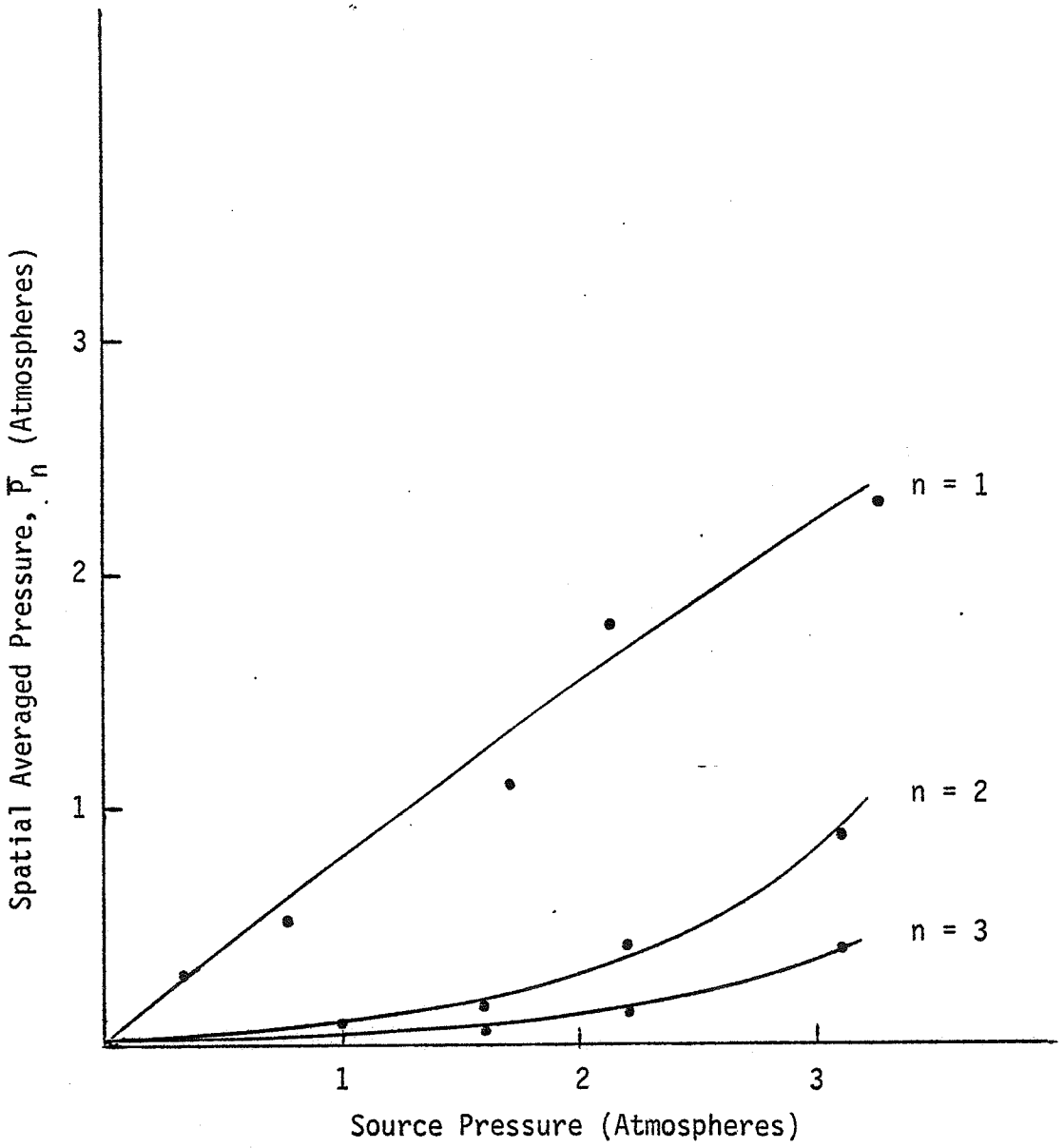

Figure 23. Spatially Averaged Harmonic Pressure Magnitude vs. Source Pressure.

amplitude effect increases with source acoustic pressure. Figure 18 shows the values of the pressure amplitude for different source levels, measured at 12 cm from the transducer. The dotted line represents a linear extrapolation of the magnitude of the fundamental, based on low amplitude measurements. As seen from the curve, the fundamental component deviated substantially from linearity as source drive was increased. The amount by which the fundamental pressure deviates from its linearly extrapolated value is plotted as amplitude of fundamental acoustic pressure/extrapolated value on Fig. 19 for different source levels. At about 1 W/cm^2 average source intensity, the deviation from linearity is about 5%. At a source level of 4.5 W/cm^2, the fundamental drops to 75% of its linear value. In terms of intensity, the fundamental has dropped to 55% of its linearly extrapolated value.

Figure 20 is a plot of the relative harmonic content P_n/P_1 for the second and third harmonics. The relative harmonic content reaches the value of one half and one third for the second and third harmonic respectively at the highest source intensity used (4.5 W/cm^2), and seems to be leveling off at that drive level.

Case II. Transaxial Measurements

To gain some insight into the spatial distribution of harmonic energy in the finite amplitude beam from a piston source, the hydrophone probe was moved perpendicular to the main axis and field plots for the first three harmonics were obtained.

Figure 21 is a sample plot of the transaxial pressure distribution

expected. In order to compare the relative harmonic content P_n/P_1 for the two cases, Fig. 23 is replotted as P_{nav}/P_{1av} vs. source pressure, as shown in Fig. 24. A comparison of Fig. 24 with Fig. 20 indicates that the spatially averaged relative harmonic content is in genaral less than the axial value. However, since the beam width of the higher harmonics is broadening with source intensity at a faster rate than the fundamental, the averaged harmonic content is closer to the axial value at higher source intensities.

Figure 24. Spatial Average Relative Harmonic Magnitude vs. Source Pressure Measured 12 cm From Source Average.

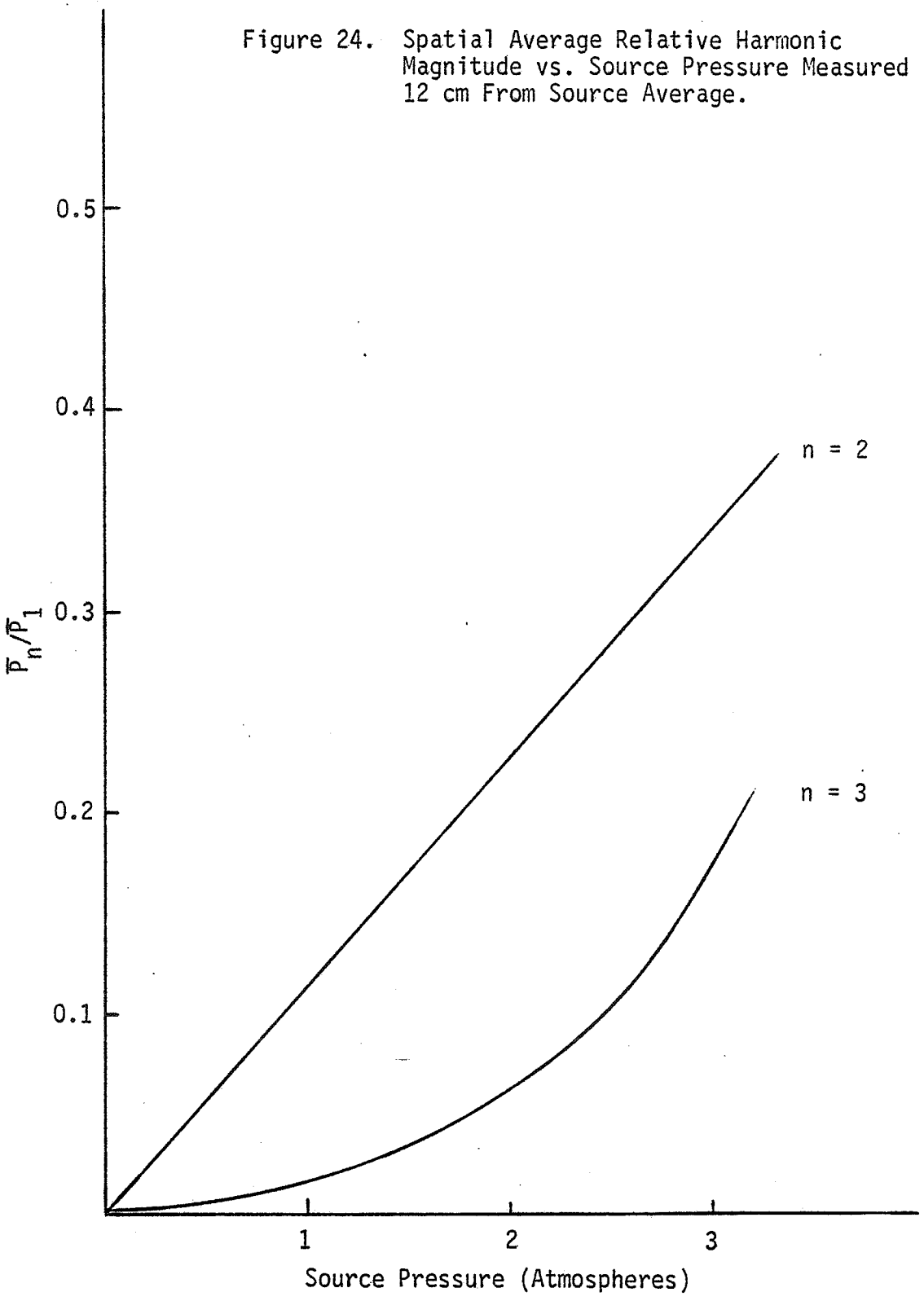

CHAPTER VI: COMPARISON WITH THEORY

It is of interest to compare the measured data with the "approximate picture" which assumed uniform plane waves. Using a B/A value of five for water, the discontinuity distance for the experimental conditions can be found (Eq. 2), as listed in Table 4.

TABLE 4

Discontinuity Distances Of The Source Levels Used

$I_o$av(W/cm^2)	$P_o$av(atm)	L(cm)
.05	.38	120
.21	.78	60
.83	1.56	30
1.62	2.2	20
3.28	3.1	15
4.55	3.7	13

Given L and the distance from the source x, one can find the harmonic magnitude based on a plane wave theory from Figs. 4 and 5 in Chapter II. The computed and measured values of relative harmonic content are plotted in Figs. 25, 26 and 27.

Figure 25 compares the harmonic content at different distances along the axis for a source pressure of 3.1 atm. Figure 26 compares the on axis harmonic content at 12 cm from the source with different source pressures, and Fig. 27 compares the spatially averaged harmonic content at the same distance. The first two comparisons (axial values) indicates that the measured harmonic content is much higher than that predicted by a plane wave theory. The third comparison indicates that the spatially averaged harmonic content agrees well with the plane wave theory except at high source pressures.

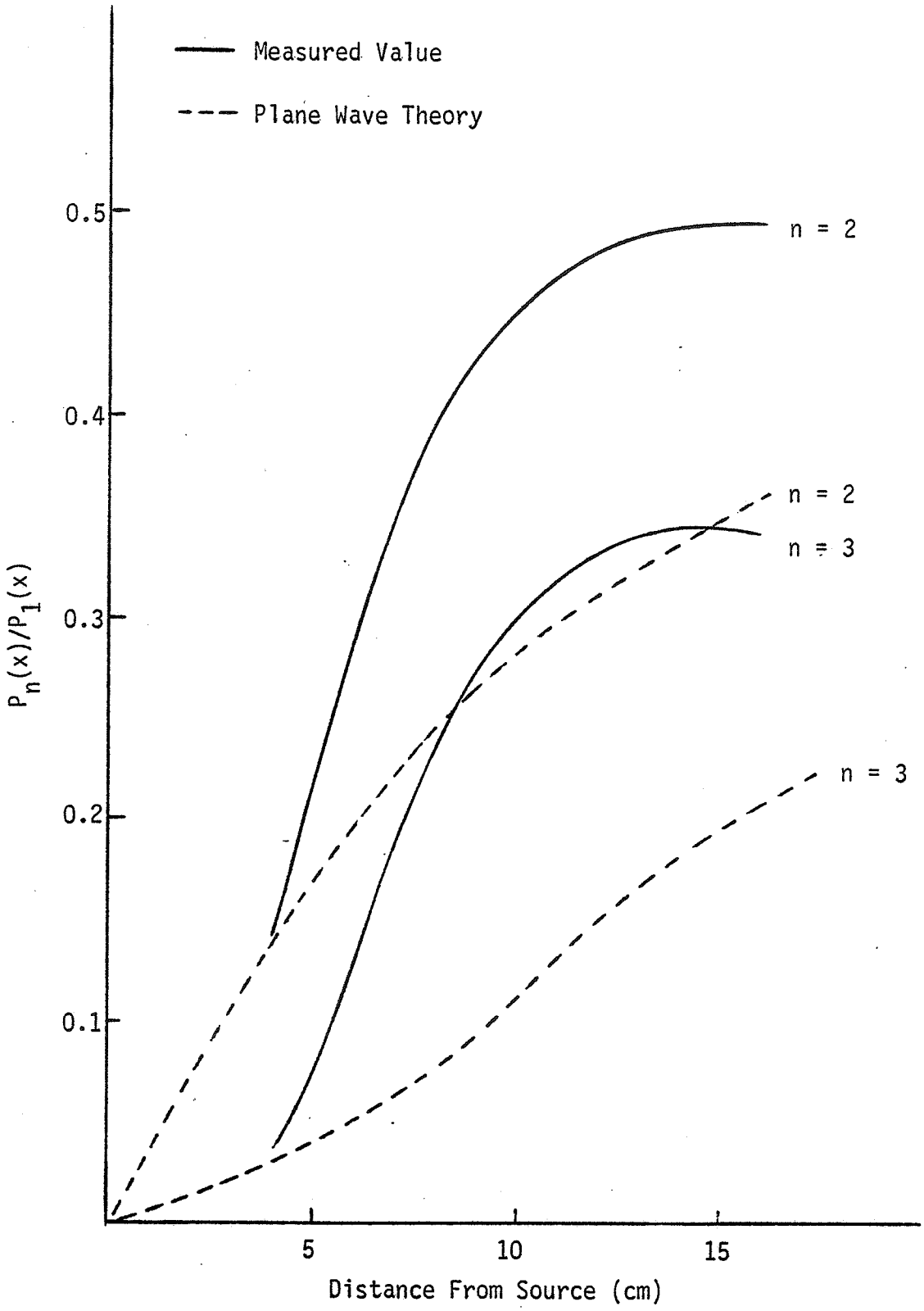

Figure 25. Comparison of Experimentally Measured Pressure Ratios To Plane Wave Theory As A Function Of Distance From The Source.

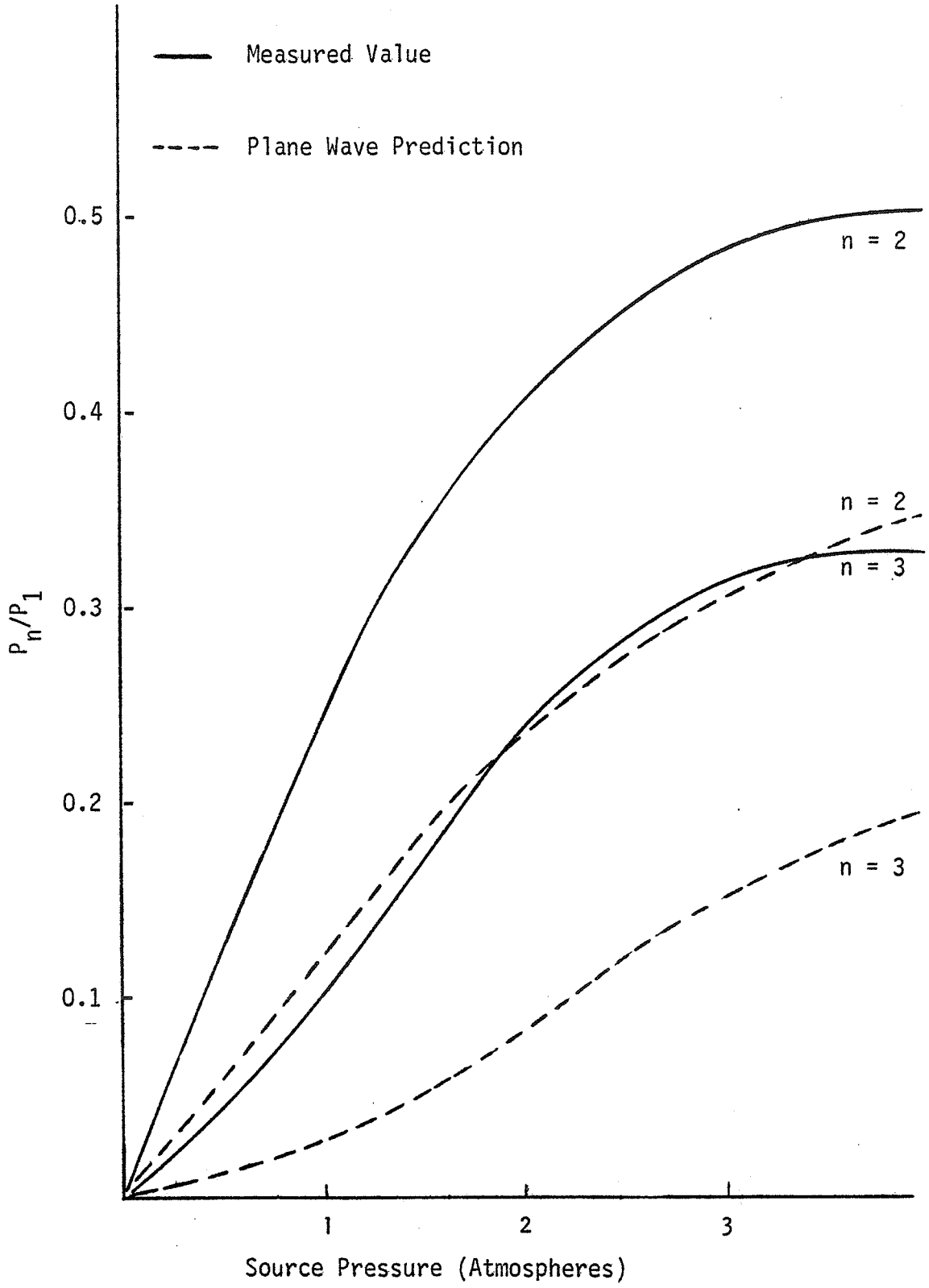

Figure 26. Comparison With Theory, Axial Value Measured At 12 cm From Source.

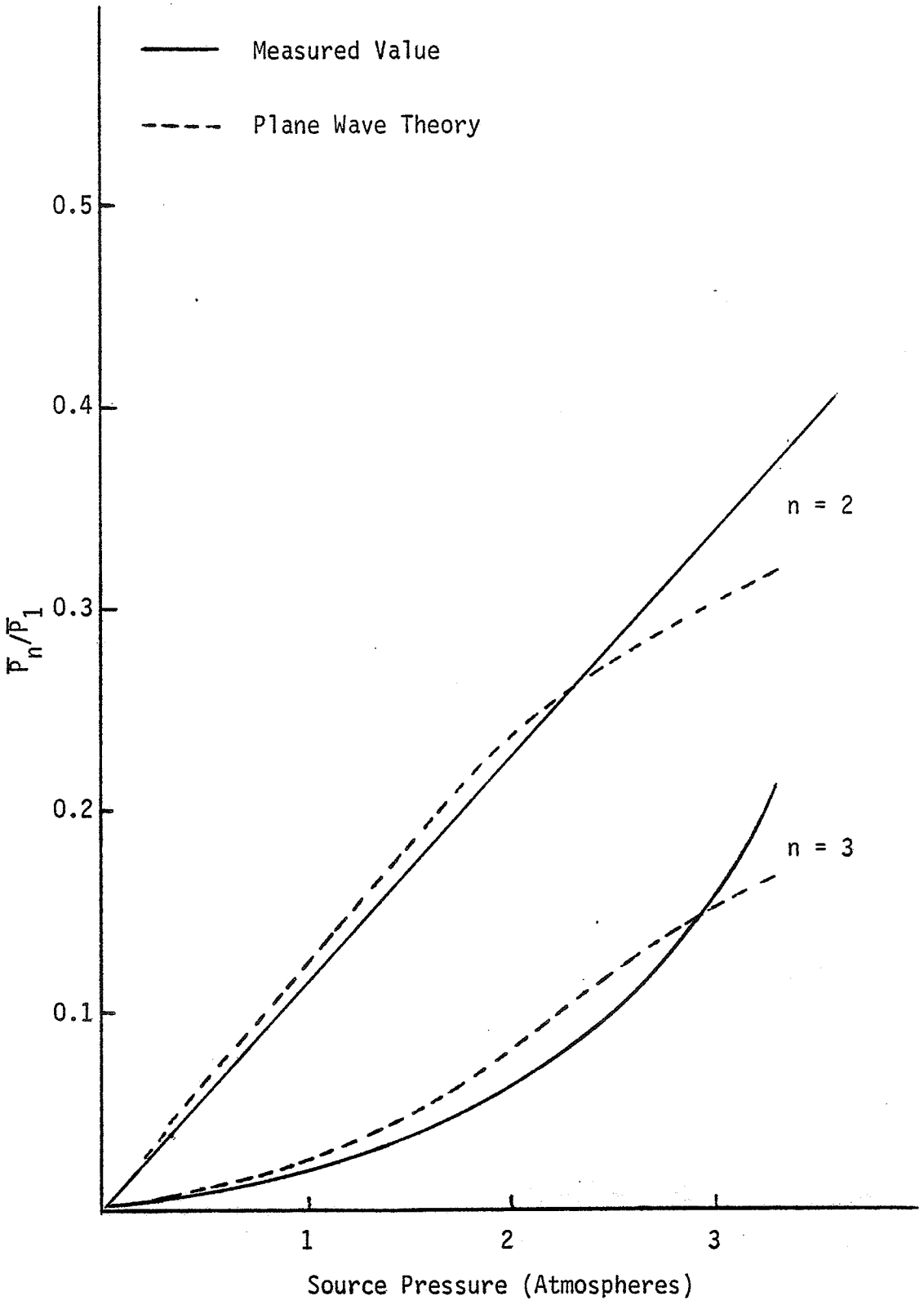

Figure 27. Comparison Of Spatial Average Pressure Ratios With Plane Wave Theory Measured At 12 cm From Source.

SUMMARY

A piezoelectric hydrophone was constructed and calibrated against a steel ball radiometer. The calibrated hydrophone was then used to measure the magnitude of the first three harmonics of the ultrasound field generated by a 3.2 MHz, ½ inch diameter plane piston source. The measurements indicate that the axial pressure of the fundamental component at the last broad maximum of the ultrasonic beam can be as much as 2.7 times that of the averaged source pressure. The axial harmonic content increases rapidly with distance and approaches that of a sawtooth wave at approximately 12 cm from the source at a moderate source intensity of 3.3 W/cm^2. The beam profiles of the three harmonics were measured at 12 cm from the source, where it was observed that the beam width of all three increased with source intensity. It was further observed that the beam width of the higher harmonics is sharper than that of the fundamental so that most of the distortion occurs near to the axis. As a result, if the harmonic was spatially averaged over an area equal to that of the source, the resulting value is less than the axial value. The spatially averaged harmonic content so obtained is found to agree with the prediction by a plane wave finite amplitude theory up to a source pressure of 2 atm. The validity of the hydrophone measurement technique was confirmed by comparing the measurements with those obtained by a filtering plate technique. The discrepancy was within 10%.

APPENDIX

RELIABILITY OF THE HYDROPHONE MEASUREMENTS

Since we did not expect the measured harmonic content to be supported by an established theory, significant conclusions were possible only after good assurance that what we measured did indeed represent the acoustic field. There are two main reasons for concern.

1. The probe was three to four fundamental wavelengths in diameter and as large as 12 wavelengths for the third harmonic. It therefore cannot be considered small compared to wavelength. The effects of reflection and diffraction caused by the probe might seriously disturb the field that was supposedly being measured.

2. The resonant frequency in the thickness mode of the probe is around 20 MHz. Near the resonant frequency, the hydrophone exhibits a drastic change in sensitivity over a small frequency range. The frequencies we were interested in were not far from that resonant frequency. Moreover, because the thickness of the receiving element is not small compared to the diameter, other modes of resonance may be present. Accordingly, rather complex responses to different frequencies might be anticipated. Since the source transducers came at fixed frequencies, it was not always possible to calibrate the hydrophone at the precise frequency desired. For example, the hydrophone probe in this research was calibrated at 6.87 MHz, but the second harmonic frequency that was measured was at 6.46 MHz, i.e. 8% lower than the calibration frequency. Therefore doubts as to the

accuracy of calibration remained. These doubts were eventually removed by tests and other observations that are now outlined:

A. Total Power Test

By the law of conservation of energy, the spatial sum of all harmonic intensities in a beam must equal the total acoustical power of the beam. The total acoustical power can be measured accurately by a radiation force method as depicted in the section on source calibration.

The spatial distribution of acoustical pressure, and hence intensity, has been measured at various levels as described previously. This intensity distribution data was spatially integrated to give the total power, and plotted against total power at the source in Fig. 28. As seen from the plot, the total power and the spatial sum of harmonic intensities agree with each other to within 10%.

B. Filtering Plate Method For Harmonic Intensity Measurements

The sound power transmission coefficient for a plate inserted in a uniform medium is given, for oblique incidence, by (Officer, Introduction to the Theory of Sound Transmission):

$$T = 4/[4\cos^2(b_2h)+(m_1+m_2)^2\sin^2(b_2h)] \qquad (8)$$

where $m_1 = \rho_2 s_2/\rho_1 s_1$, $m_2 = 1/m_1$, $s_1 = c_1/\cos\theta_1$, $s_2 = c_2/\cos\theta_2$, $b_2 = 2\pi f/s_2$, and $\sin\theta_1/\sin\theta_2 = c_1/c_2$. ρ_1, c_1, ρ_2, c_2 are respectively the density and velocity of the medium and the plate. θ_1 and θ_2 are

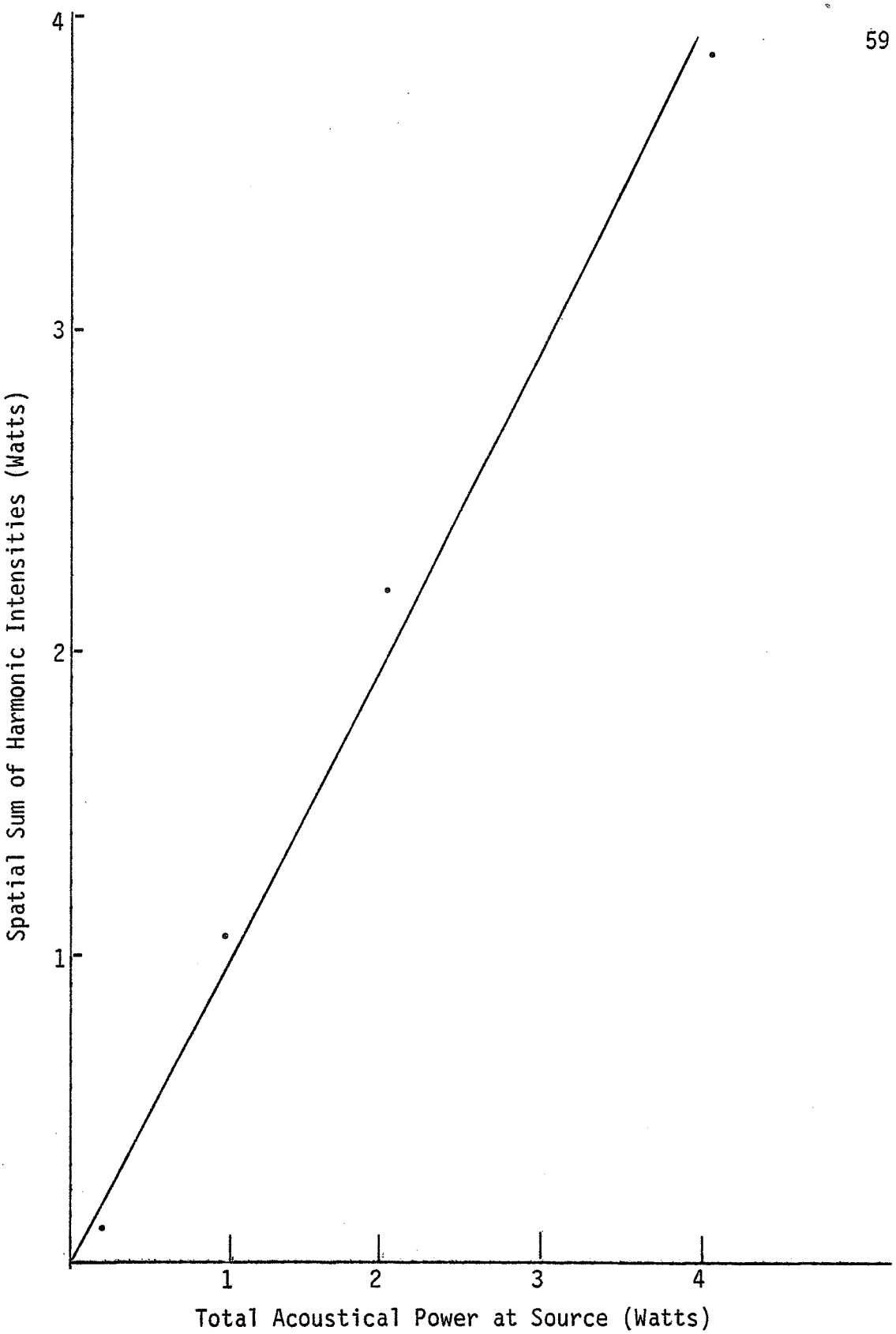

Figure 28. Spatial Sum of Harmonic Intensities vs. Total Acoustical Power at the Source,

respectively the angle of incidence to the plate and the angle of refraction in the plate.

If the wave is incident normally to the plate, and if the plate thickness is half a wavelength of the second harmonic, the plate will provide perfect transmission for the second harmonic and have maximal attenuation to the fundamental and the third harmonic. The transmission coefficient for such a plate is depicted in Fig. 29 for materials of different acoustical impedances. However, if the plate is rotated so that the wave is incident at an angle θ with the normal, the frequency of maximal transmission is shifted upward according to Eq.8. This predicted shift in pass frequency with θ is plotted in Fig. 30. Thus by rotating the plate, one can tune the filter plate to the frequency of interest.

In order to reduce the effect of reflection from the filtering plate, the source was pulsed to give 30 μsec on time and 150 μsec off time. An aluminum plate 0.510 mm thick was used as the filtering plate. A 1/16" diameter steel ball was suspended behind the plate for intensity measurements.

The filter plate was rotated until a maximum in deflection of the steel ball was observed. Since the steel ball radiomater requires at least ¼ W/cm^2 for accurate measurements, a peak source intensity of 3.3 W/cm^2 was required to generate sufficient second harmonic intensity for deflection.

After intensity measurements, the steel ball was replaced by a hydrophone and the transmission coefficient of the plate to the three

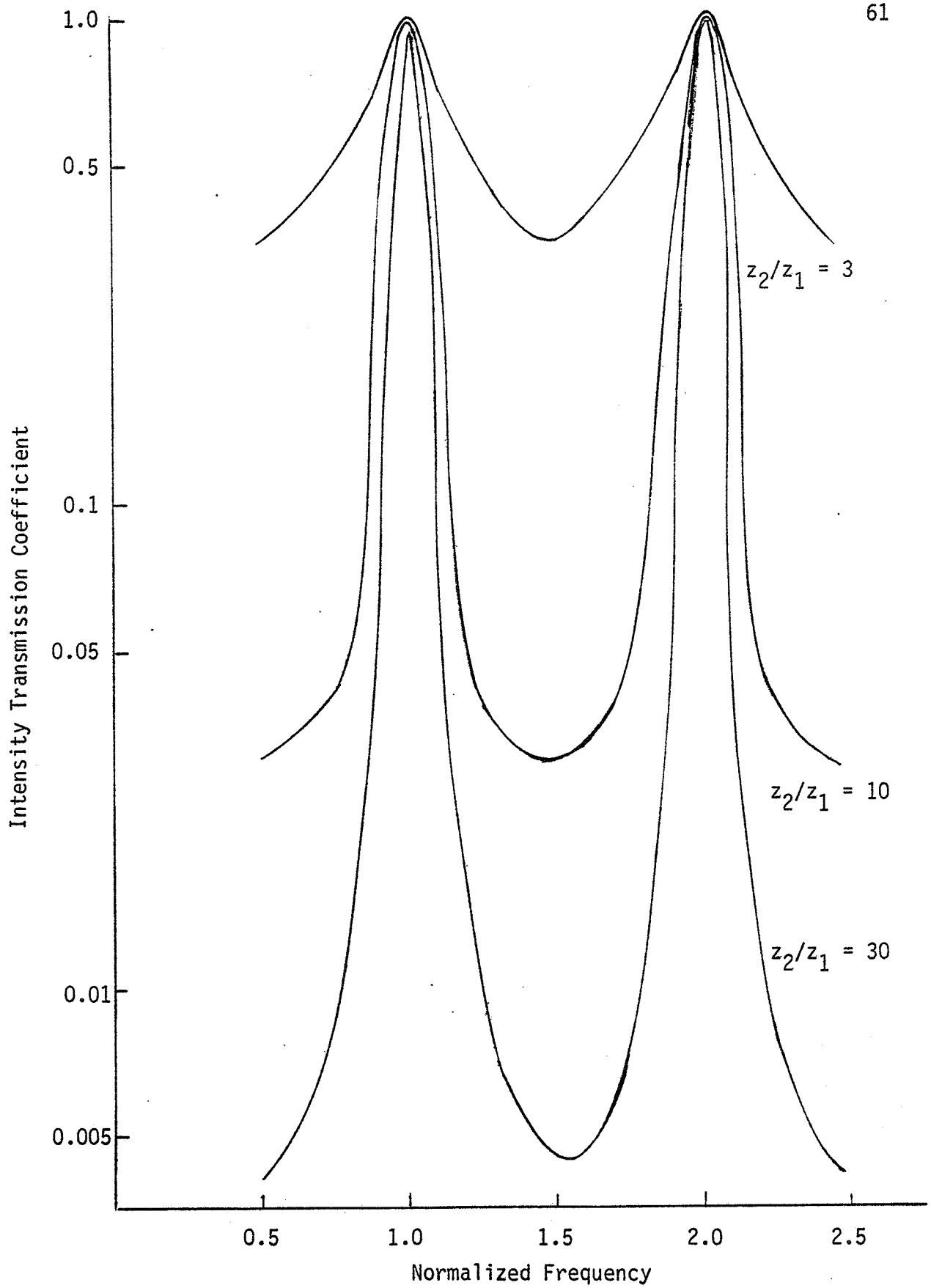

Figure 29. Sound Power Transmission Through a Half Wavelength Plate at Normal Incidence.

Figure 30. Pass Frequency of Filtering Plate vs. Angle of Incidence.

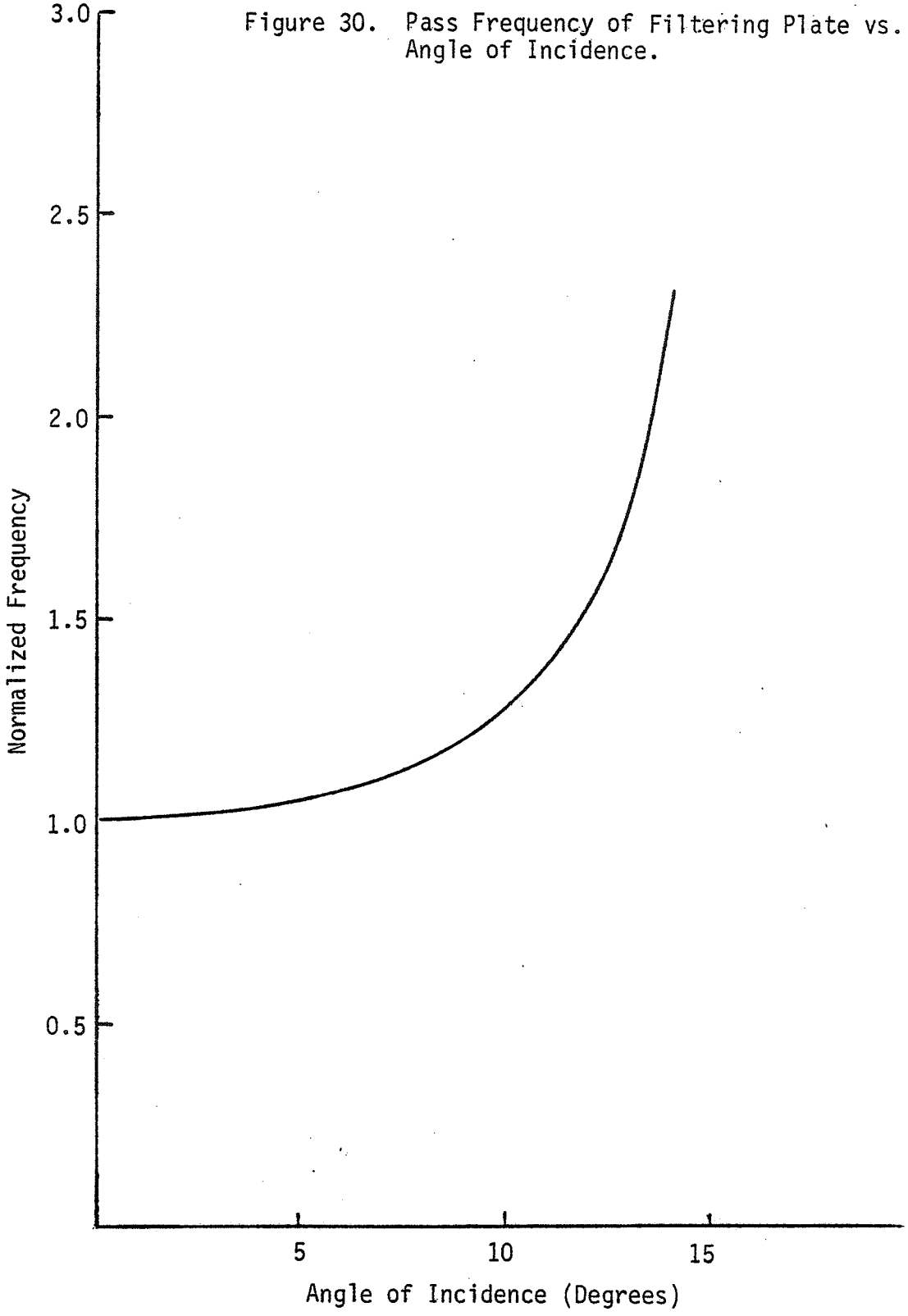

different harmonics was measured by comparing the harmonic magnitudes with and without the plate. The intensity transmission coefficient, defined as (Pressure magnitude behind the plate/Pressure magnitude without the plate)^2 is listed in Table 5 for the three harmonic frequencies.

TABLE 5

Intensity Transmission Coefficient Of Filtering Plate

Frequency	Intensity Transmission Coefficient
3.23 MHz	.028
6.46 MHz	.774
9.69 MHz	.046

As seen from the table, about 3% of the fundamental and 5% of the third harmonic were able to pass the filter plate. The intensity measured with the ball behind the filtering plate is therefore a sum of harmonic intensities. If we neglect harmonics higher than the third, the intensity measured with the ball can be expressed as $I_{measured} = I_1(.028) + I_2(.774) + I_3(.046)$ where I_1, I_2 and I_3 are intensities of the three harmonics incident upon the filter plate. I_1 and I_3 can be estimated by hydrophone measurements. With I_1, I_3 and $I_{measured}$ known, I_2 can be computed. The second harmonic intensity

obtained by this technique was compared with hydrophone measurements made previously. The agreement was within 15%. In terms of pressure measurements, the agreement would be about 7.5%, well within the accuracy of the measurement methods.

REFERENCES

Beyer, R.T., Nonlinear Acoustics, pp. 91-164. Naval ship systems command, Department of the Navy, Washington, D.C. (1964).

Blackstock, D. T., "Connection between the Jay and Fubini solutions for plane waves of finite amplitude." JASA 39, pp. 1029-1026 (1966).

Blackstock, D. T., "Thermoviscous attenuation of plane, periodic, finite amplitude waves." JASA 36, pp. 534-542 (1964).

Carstensen, E. L., Law, W. K. and McKay, N. D., "Demonstration of nonlinear acoustical effects at biomedical frequencies and intensities." To be published.

Cook, B. D., "New Procedures for Computing Finite Amplitude Distortion." JASA 34, p. 941 (1962).

Dunn, F., Averbuch, A. J. and O'Brien, Jr., W. D., "A primary method for the determination of ultrasonic intensity with the elastic sphere radiometer." Acoustica 38, p. 58 (1977).

Fry, W. J. and Dunn, F., Physical techniques in biological research, Vol. 4, Ch. 6, Academic Press, N.Y. (1962).

Gould, R. K., Smith, C. W., Williams, Jr., A. D. and Ryan, R. P., "Measured structure of harmonics self generated in an acoustic beam." JASA 40, pp. 421-427 (1966).

Hasegawa, T. and Yosioka, K., "Acoustic-radiation force and a solid elastic sphere." JASA 46, p. 1139 (1969).

Ingenito, F. and William, Jr., A. O., "Calculation of second harmonic generation in a piston beam." JASA 49, p. 320 (1971).

Keck, W. and Beyer, R. T., Phys. Fluids 3, pp. 346-352 (1960).

Kinsler and Frey, Fundamentals of acoustics, Ch. 7, Wiley and Sons, 1962.

Krasilnikov, V. A., Shklovskaya-Kovdy, V. V. and Zarembo, L. K., "On the propagation of ultrasonic waves of finite amplitude in liquids." JASA 27, pp. 642-647 (1957).

Lockwood, J. C., Muir, T. G. and Blackstock, D. T., "Directive harmonic generation on the radiation field of a circular piston." JASA 53, pp. 1148-1153 (1973).

Muir, T. G. and Carstensen, E. L., "Prediction of non-linear acoustic effects at biomedical frequencies and outer sites." To be published.

Officer, Introduction to the Theory of Sound Transmission.

Rudenko, O. V. and Soluyan, S. I., Theoretical Foundation of non-linear Acoustics. (translated from the Russian), Plenum Press, N.Y. (1977).

Ryan, R. P., Lutsch, A. and Beyer, R.T., "Measurement of the distortion of finite ultrasonic waves in liquids by a pulse method." JASA 34, pp. 31-35 (1962).

Shooter, J. A., Muir, T. G. and Blackstock, D. T., "Acoustic saturation of spherical waves in water." JASA 55, pp. 54-62 (1974).

Smith, C. W. and Beyer, R. T., "Ultrasonic radiation field of a focusing spherical source at finite amplitudes." JASA 46, pp. 806-813 (1969).